Seasonal performance of a novel solar-assisted dual source multifunctional heat pump: a field study

Giorgio Besagni[1,*], Lorenzo Croci[1], Riccardo Nesa[1,2], Luca Molinaroli[2]

[1] Ricerca sul Sistema Energetico - RSE S.p.A., Power System Development Department, via Rubattino 54, 20134 Milano (Italy)

[2] Politecnico di Milano, Department of Energy, via Lambruschini 4a, 20156, Milano (Italy)

Corresponding author: Giorgio Besagni, Ricerca sul Sistema Energetico - RSE S.p.A., Power System Development Department, via Rubattino 54, 20134 Milano (Italy) – email: giorgio.besagni@rse-web.it; tel: +39 0239925078.

Abstract

The integration between heat pumps and renewable energy sources is a recognized strategy to be pursued to reduce primary energy consumption. This paper contributes to the existing discussion on solar assisted heat pumps, for heating and cooling applications, and for the production of domestic how water. In particular, this paper presents the results of a field study concerning a novel solar-assisted dual-source multifunctional heat pump, installed in a detached house in Milan. The proposed system couples hybrid photovoltaic/thermal (PVT) panels with a multifunctional and reversible heat pump. The heat pump is equipped with an "*air-source*" evaporator and a "*water-source*" evaporator, connected in series and operated alternatively, based on the ambient conditions, system parameters and operating modes. The PVT panels are connected with the heat pump by two storage tanks to be used to produce domestic hot water and to be used in "*water-source*" evaporator. The proposed system has been tested experimentally; the results show that the system was able to maintain high efficiency in the different seasons and was able to produce domestic hot water. It was found that the use of the "*water-source*" evaporator allowed to significantly increase the performance of the system and to avoid the defrost cycles.

Keywords: Solar assisted heat pump, Hybrid photovoltaic/thermal panels, Dual Source system, Heat Pump, Field trial, Energy efficiency

Nomenclature and abbreviation list

Acronyms

COP	Coefficient Of Performance
COP_{fl}	full load efficiency in Eq. (15)
DHW	Domestic Hot Water
DOF	Degradation coefficient due to defrost operations in Eq. (15)
EER	Energy Efficiency Ratio
HP	Heat Pump
PV	Photovoltaic
PCM	Phase Change Material
PLF	Part Load Factor in Eq. (15)
PVT	Hybrid thermal-photovoltaic
SAHP	Solar-Assisted-Heat Pump

Symbols

c_p	Specific heat capacity of water	[kJ/kg K]
$En_{HP \rightarrow DWH\text{-}tank}$	Energy transferred from the heat pump to the *DHW* tank	[kWh]
$En_{PVT \rightarrow DWH\text{-}tank}$	Energy transferred from the PVT panels to the *DHW* tank	[kWh]
m	Mass flow rate	[kg/s]
N	Time discretization in Eq. (4)	[-]
$\dot{Q}$	Heat transfer rate from the heat pump to the *DHW* tank	[kW]
	Heat transfer rate from the PVT panels to the *DHW* tank	[kW]
	Heat transfer rate from the heat pump to the fan-coils	[kW]
T	Temperature	[°C]
t	Time in Eq. (4)	[min]
$V_{DHW,tank}$	Volume of the *DHW* storage tank	[m^3]
$V_{DHW,tank}$	Volume of the *"intermediate-temperature"* storage tank	[m^3]
ρ	Density of water	[m^3/kg]
η	Efficiency	[-]

Subscripts

amb	Ambient conditions
el	Electrical energy

eva	Evaporator
inlet	Inlet condition
outlet	Outlet condition
PV	Photovoltaic panels
PVT	Hybrid thermal-photovoltaic panels
th	Thermal energy

1 Introduction

Energy efficiency and the use of renewable energy sources are key goals of European energy policies, to achieve a sustainable future [1]. The 2007 Climate and Energy package foresaw, considering the 2020 target and the 1990 situation, (a) a 20% reduction of primary energy consumption in buildings, (b) a 20% increase of renewable energy production, and (c) a 20% decrease of greenhouse gas emissions. These targets were updated by the 2030 Climate & Energy framework, aiming to reduce (a) the greenhouse gas emissions at 40%, (b) the share for renewable energy at 27% and (c) improvement in energy efficiency at 27%. Within these requirements, large attention is devoted to the heating/cooling sections and to buildings, owing to their large energy consumption (i.e., in Europe buildings consume approximately 40% of the primary energy); in this respect the reader should refer to the Energy Performance of Buildings Directive (EPBD, Directive 2002/91/EC, ref. [2]), and its recast (EPBD recast, Directive 2010/31/EC, ref. [3])[1]. Generally, in heating/cooling sections and in buildings, the above-mentioned targets can be achieved by acting on the demand side (i.e., retrofitting the building stock, see refs. [4, 5]) and/or by acting on the supply side (i.e., new heat supply technologies, see ref. [6]); the two sides are highly correlated and their synergy was studied within the heat roadmap Europe studies (see refs. [7, 8]). On the practical point of view, considering the heating/cooling supplies side, the integration between heat pumps and renewable energy sources is a promising technology to meet the above-mentioned requirements. It is worth noting that the application of renewable energy-based heat pumps are achieving a growing interest when considering the broader framework of the heating sector. For example, in the heat roadmap Europe studies, it has been estimated a potential increase of the district heating share to 50% of the entire heat demand by 2050, with approximately 25–30% of it being supplied using large-scale electric heat pumps: this increase enables a large utilization of alternative sources of heat, as renewable sources. Taking into account the above-mentioned policy and technology framework, this paper contributes to the broader discussion on innovative renewable energy-based heat pumps. In the following of the introduction, a brief literature survey and an overview of the technology is proposed to fit the present paper within the present body of knowledge and to clearly define the specific contribution of this paper within the state-of-the-art of solar-assisted heat pump technologies.

[1] These documents devoted large attention in discussing the implementation of nearly zero energy buildings In particular, Article 9 of the EPBDrecast states that MS shall ensure that new buildings occupied by public authorities and properties shall be NZEBs by December 31,2018 and that new buildings shall be nearly zero energy buildings by December 31, 2020

Within the heating and the cooling sectors, heat pumps are among the most interesting solutions and they can represent a valid alternative to conventional systems, because they use less primary energy. In this respect, multifunctional heat pumps can be applied not only for heating and cooling applications, but also for the production of domestic hot water (*DHW*), by exploiting different heat sources (i.e., ground-source, air-source or water-source). However, there is still a great uncertainty concerning their consumptions in large-scale applications, as field measurements of real installations often have shown lower efficiencies compared with laboratory-scale experimentations [9]. Indeed, the performances of heat pumps are largely influenced by the boundary conditions and the operating conditions of the system (i.e., heat source temperature, outlet fluid temperature, thermal load, …). In particular, the coefficient of performance (*COP*) of air-source heat pumps depends on the ambient temperature, T_{amb} (viz. T_{amb} is related to the evaporating temperature, T_{eva}). As a consequence, in the winter season, when heating is needed and T_{amb} is lower, the system performance decreases, owing to the lower evaporating temperature. Conversely, considering a reversible heat pump in the summer season, when cooling is needed and T_{amb} is higher, the system performance decreases, owing to the higher condensing temperature. In addition, when an air-source heat pump operates in heating mode, frost can be formed on the evaporator surface. This phenomenon occurs when the surface temperature is both below the freezing point of water and the dew point of the moist air. In this situation, the frost acts as a thermal insulator and, in addition, reduces the airflow passage area; therefore the accumulated frost leads to a decrease in the performance, owing to the decrease in the evaporating temperature. Hence, a periodic defrosting is needed and, nowadays, the most widespread defrost method is reverse-cycle defrost [10]: the refrigerant flow is reversed and hot vapor from compressor flows through the outdoor coil melting the frost[2]. It follows a drop of hourly *COP* because of compressor consumptions while no space heating is provided. For example, Madonna and Bazzocchi [11] reported, from experimental field tests, that *COP* decreased by 13% and 23% in the case of 1 or 2 defrost cycles per hour, respectively. This issue works critically for air-source heat pumps, especially when employed in cold climates [12, 13, 14].

In this respect, the coupling between solar technologies and heat pumps—"*solar-assisted heat pumps*" (*SAHPs*)—is a promising technology to overcome the above-mentioned limitations, to reduce the consumption of energy resources, to meet the targets set by the recent regulations and to foster the spread of air-source

[2] During a defrost cycle heat is taken from the inside of the building to defrost the outdoor coil, as a consequence, when defrost cycles occurs, the hourly thermal energy that a unit can provide is reduced.

heat pumps in cold climates. The SAHP concept has been firstly proposed by Sporn and Ambrose [15] and, subsequently, it has been widely studied; in particular, to further expand the application area and improve the efficiency of the heat pumps, different researchers investigated multi-functional heat pumps to produce both space heating/cooling and *DHW* production (see the survey of Cai et al. [16]). Generally speaking, heat pumps can be coupled with photovoltaic (*PV*) panels, thermal collectors or hybrid photovoltaic/thermal (*PVT*) panels, as outlined in the literature surveys proposed by Kamel et al. [17] and by Mohantaj et al. [18]. In practical applications, heat pumps are integrated with thermal or *PVT* panels, in direct- expansion or indirect-expansion configurations. In direct-expansion *SAHP*, the solar panel corresponds to the evaporator of heat pump (see, for example, the early study of Huang and Chyng [19], who presented a *SAHP* for *DHW* production, or the more recent study of Amin and Hawlader [20], who presented a *SAHP*–based desalination system for *DHW* production); conversely, in indirect-expansion *SAHP*, an intermediate heat exchanger is used to couple the solar system with the heat pump (see, for example, the study of Cai et al. [16]). The reader should refer to some of the recent review papers for a detailed comparison between advances and disadvantages of the two configurations [17]. In addition, *SAHP* can be classified into three sub-categories: (a) parallel systems, (b) series systems and (c) dual-source systems. In parallel systems, the heat pump receives energy from the ambient, and the solar energy is supplied directly for either space heating or for *DHW* production. In series systems, solar energy is supplied to the evaporator of the heat pump, thus raising the evaporating temperature (thus, increasing the *COP*) and cooling the solar collectors (thus, increasing the efficiency of the solar panels; see refs. [21, 22, 23]). In the dual-source systems, the evaporator can receive energy from either the atmosphere or from the solar energy, depending on the ambient conditions and system operation .

In this complex framework, this paper contributes to the existing discussion concerning multifunctional *SAHP* for heating and cooling applications, as well as for the production of *DHW*. In the last decades, different systems have been proposed and, in the following, a brief literature survey is proposed to better outline the particular framework of this research. Wang et al. [24] experimentally investigated, in a laboratory-scale experimental setup, an indirect dual-source ("*air-source*" and "*water-source*" evaporators) *SAHP* for space heating and cooling and water heating. A storage tank, connected to thermal panels, was used to supply heat to the "*water-source*" evaporator or to produce *DHW*. They reported *COP* = 4, in the heating mode. Bridgeman and Harrison [25] experimentally investigated, in a laboratory-scale experimental setup, the performance of an indirect series *SAHP* for water heating. They observed *COP* = 2.8 – 3.3, depending on the evaporator and

condenser temperatures. Loose et al. [26] performed field tests of various combined *SAHP* systems with different heat sources, for space heating and water heating. The system employed solar thermal collectors and geothermal heat pump with borehole heat exchangers. The collectors fed the storage tank directly when the sufficient solar radiation was available. Otherwise, low grade energy from the collectors would be used in the heat pump for space heating. Bakirci et al. [13] investigated the performance of an indirect SAHP system for space heating. The solar collectors directly charged a storage tank which was linked to an evaporator to provide a heat source for the heat pump. They observed *COP* in the range of 3.3 – 3.8. Bai et al. [27] theoretically studied, by using a TRNSYS model, an indirect combined hybrid *PVT SAHP* system for *DHW* production. Year round performance results were simulated under the different climatic conditions (Hong Kong and different locations in France) and an average *COP* = 4.9 has been observed. Keliang et al. studied a direct expansion *SAHP* by a numerical approach (viz. a distributed-parameter-modelling); their results clearly demonstrated the importance of variable speed compressor to modulate the capacity supplied and adapt to the operating conditions. Lv et al. [28] theoretically studied a dual-source auto-cascade SAHP operated with the zeotropic mixture R32/R290 for *DHW* production and studied its performance by using a lumped-parameter model. They observed *COP* in the range of 4.0 – 3.8; however, the performance of the system are highly dependant on the mixture composition and, thus, this solution requires further research before large-scale applications. Jie et at al. [29] and, later Cai et al. [16] studied an indirect multifunctional *SAHP* by experimental and numerical approaches; the experimental approach has been used to validate the numerical approach. Subsequently, the numerical approach has been used to perform sensitivity analysis and they observed *COP* in the range of 2.7 – 2.2.

From the above-mentioned literature survey, as well as from the previous literature surveys [30, 31, 32, 33, 16], it is observed that there is a lack of field studies concerning practical demonstration and fields studies concerning multifunctional dual-source ("*air-source*" and "*water-source*" evaporators) *SAHP*. For example, Cai et al. [16], in their recent study, stated that "*few theoretical study of the solar-assisted multi-functional heat pump has been conducted and the related experimental verifications are still insufficient*". In addition, as remarked by Croci et al. [34], most of the studies focused on the application in cold climates and there is a lack of studies concerning a technical solution that may be feasible, in the whole year, in Mediterranean area. To this end, this paper presents a novel solar-assisted dual-source multifunctional heat pump (installed in a detached house in Milan) and discusses the results of a field study. It is worth noting that the Milan area is

characterized by a peculiar climate (cold and humid winter and hot summer) and, thus, this study further contribute to the existing discussion on the application of heat pumps in the Mediterranean area. The proposed study is the preliminary step towards future studies concerning the optimization of the systems by using an integrated numerical-experimental approach (in this respect, the reader may refer to the procedure proposed by Chen et al. [35]).

The paper is organized as follows. First, the experimental setup and methods are presented and described; second, the experimental results are commented and discussed; subsequently, the proposed solar-assisted dual source multifunctional heat pump is compared with an air-to-water single-source multifunctional heat pump; finally, main conclusions are drawn

2 Experimental setup and methods

In this section, the experimental setup and the experimental methods are described. First, the multifunctional heat pump system and the main characteristic of the components are presented (Section 2.1). Second, the details concerning the operation procedures are outlined (Section 2.2). Finally, the experimental techniques (Section 2.3) and the performance parameters (Section 2.4) are described.

2.1 Experimental setup

The multifunctional heat pump system (Figure 1) was designed and installed in a detached house (Figure 2) located in Milan, at RSE Spa[3] headquarter (Latitude 45.47°, Longitude 9.25°), located near Milano Linate, which is generally used as reference for climatic conditions in the Milan area. It is worth noting that the Milan area is characterized by a peculiar climate (cold and humid winter and hot summer). The interested reader may refer to the discussion proposed by Rosa et al. [36] for a detailed analysis and comparison of the historical trends of heating and cooling degree days in different cities in Italy; they concluded that Milan can be considered among the coldest climatic conditions in the winter period (along with high humidity, which works critically for the heat pump working conditions). For this reason, the proposed study also contributed to the existing discussion on the application of *SAHPs* in cold climates. The detached house consists of a prefabricated house with an

3 RSE Spa carries out research into the field of electrical energy with special focus on national strategic projects funded through the Fund for Research into Electrical Systems. The activity covers the entire supply system with an application-oriented, experimental and system-based approach.

heating/cooling area equal to 60 m^2, divided in four rooms simulating a living room, a kitchen, a bedroom and a bathroom. The house is equipped with five fan coils used for space heating/cooling and has a nominal heating load equal to 4 kW_{th} (indoor temperature equal to 20 °C and outdoor temperature equal to -5 °C). Bazzocchi and Madonna [11] reported additional information concerning the detached house and are briefly summarized in the following: (a) the opaque walls are of glass wool and wood with an U-value of 0.59 W/m^2K; (b) the U-value of the floor and of the ceiling are of 0.58 W/m^2K and 0.54 W/m^2K respectively; (c) the windows (U-value of 2.92 W/m_2K) are double glazing with metal frames and covers a total surface of 5 m^2.

Figure 1 displays the layout of the multifunctional heat pump, which is composed by five parts: (a) a solar system, (b) a *DHW* storage tank and an "*intermediate-temperature*" storage tank, (c) a reversible heat pump, (d) terminal of the heating and cooling systems (viz. fan coils) and (e) circulating pumps (Table 1). Further details concerning the different components of the system are provided in the following. The proposed system couples hybrid photovoltaic/thermal (PVT) panels with a multifunctional and reversible heat pump. The heat pump is equipped with an "*air-source*" evaporator and a "*water-source*" evaporator, connected in series and operated alternatively, based on the ambient conditions, system parameters and operating modes. The PVT panels are connected with the heat pump by two storage tanks to be used to produce domestic hot water and to be used in "*water-source*" evaporator. Based on the operating conditions, the hot water is sent to one of the storage tank. In the following, the main components of the system are described.

Solar system. The solar system consists of seven *PVT* panels and a *PV* panel (Figure 2). The *PV* panel has the same size and cells characteristic of the *PVT* panels, to compare the performance of the two technologies. The seven *PVT* panels (south-oriented, 45° titled angle) have 1.75 kW_{el} nominal power and are of the roll-bond technology (Figure 3a). They are composed by polycrystalline silicon cells, a steel heat-exchanger and a 0.02 m insulation. Figure 4 displays further details of the PVT panels and Table 2 and Table 3 collect their technical information. To prevent icing-related issues in the hydronic loop of the PVT collectors, water/ethylene glycol with a nominal flow rate equal to 0.630 m3/h was used.

Storage tanks. The *DHW* storage tank (0.186 m^3 in volume) was used to produce hot water; conversely, the "*intermediate-temperature*" storage tank (0.300 m^3 in volume, Figure 3b) was used as "*water-source*" from the heat pump, instead of the "*air-source*" one, to improve the performance in cold days and avoid defrosts and reduce temperature fluctuations. The "*intermediate-temperature*" storage tank is connected to the heat pump, by a plate heat exchanger (Figure 3c) and the maximum flow rate towards the "*water-source*" heat

195 exchanger is 1.45 m^3/h.

196 **Heat pump unit.** The heat pump is an ad-hoc modified version of the *Clivet GAIA 31*. In particular, it is a R410A
197 (total refrigerant charge = 6.9 kg) reversible heat pump, 6.8 kW_{th} nominal heating capacity and 3.47 nominal
198 COP (water leaving temperature equal to 35 °C, dry-bulb temperature equal to 7 °C, and wet-bulb equal to 6
199 °C). The compressor is a variable speed twin rotary compressor which allows to modulate the capacity
200 supplied[4], and the defrost method is the reverse-cycle defrost. The machine is equipped with an electronic
201 expansion valve used to keep the superheating at evaporator outlet to 5 °C. The advantages of variable-
202 frequency compressors and electronic expansion valves have been discussed by Keliang et al. [37], to whom
203 the reader should refer.

204 **Circulating pumps.** As shown in Figure 1, the experimental system includes circulating loops: (a) solar collector
205 loops; (b) "*intermediate-temperature*" storage tank to heat pump; (c) indoor terminal fan-coil side loop and (d)
206 *DHW* circulating loops (not shown in figure 1, located between the heat pump and the DHW storage system,
207 *P4*). Photos of the circulating pumps are provided in Figure 3d. It is worth noting that pumps *P1*, *P2* and *P3* are
208 controlled by changing their rotation speed. The technical details of the different pumps used are provided in
209 Table 1. It is worth noting that the use of the "*air-source*" evaporator automatically deactivate pump *P2*.

210 **Table 1. Details on circulating pumps used**

Code	Location (Figure 1)	Technical details	Power [W]
P1	Solar circulating pump	DEB Evolplus Small 60/180 M PWM	5 ÷ 100
P2	"*intermediate temperature*" circulating pump	WILO Stratos Para 25/1-7 PWM	5 ÷ 70
P3	Fan-coil circulating pump	WILO Stratos TEC RS 25/7 PWM	3 ÷ 70
P4	*DHW* circulating pump	WILO ZRS 12/7	86 (fixed speed)

211

[4] It is worth noting that, a variable speed compressor, beside being able to modulate the capacity supplied, reduced the losses due to On/Off behaviour (i.e., Cycling losses). For further details the reader should refer to ref. [34].

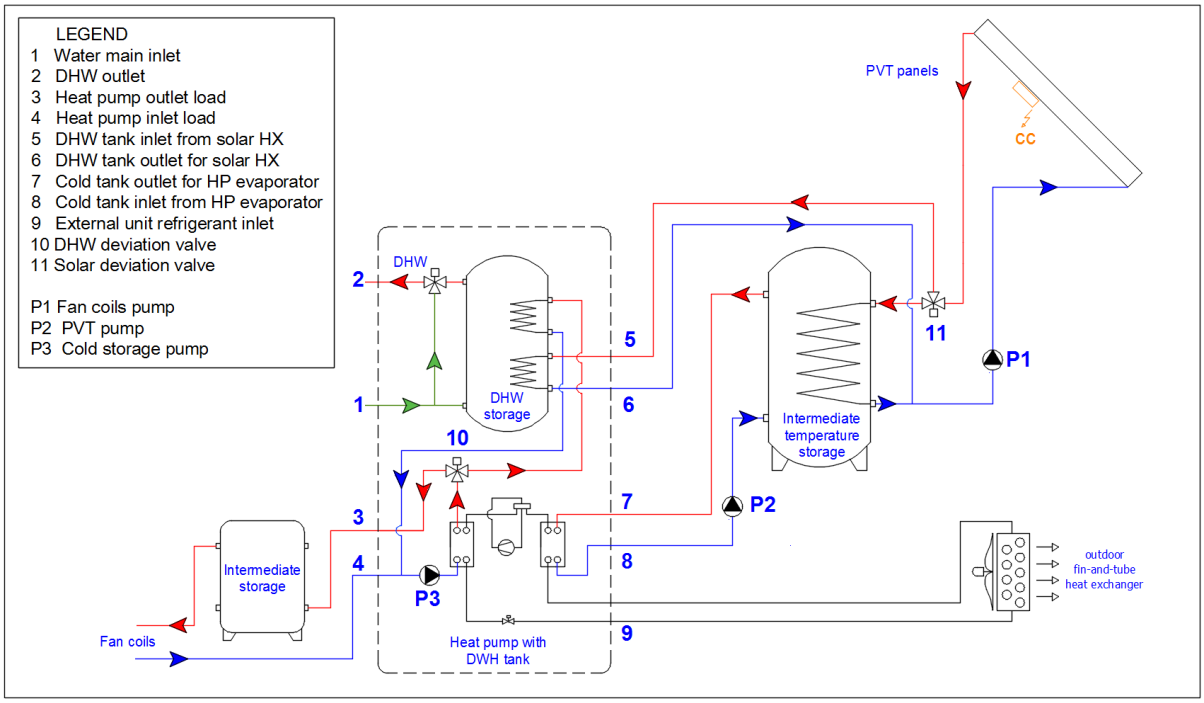

Figure 1: Experimental layout

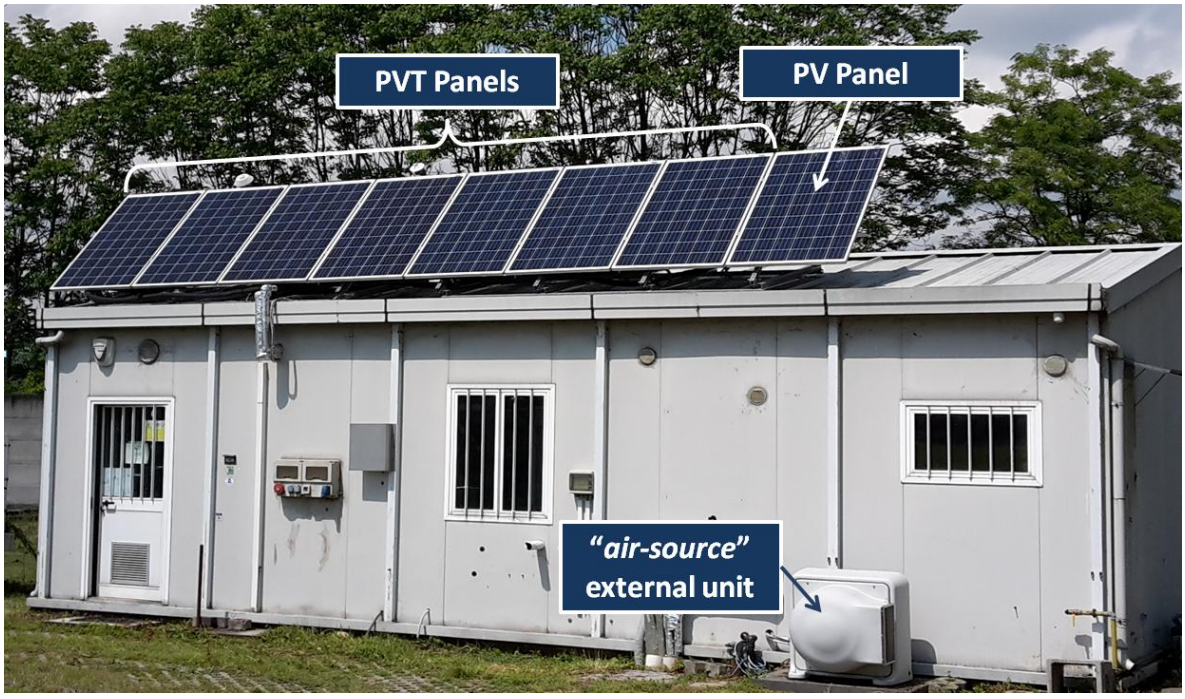

Figure 2: Photo of the detached house

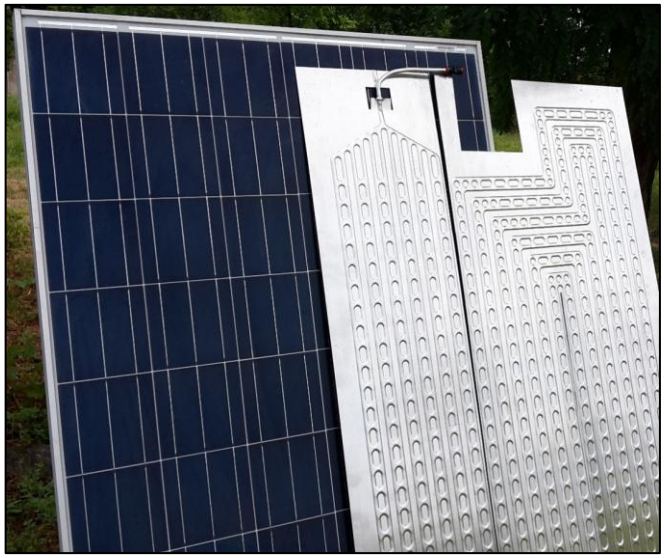

(a) PVT roll-bond panels

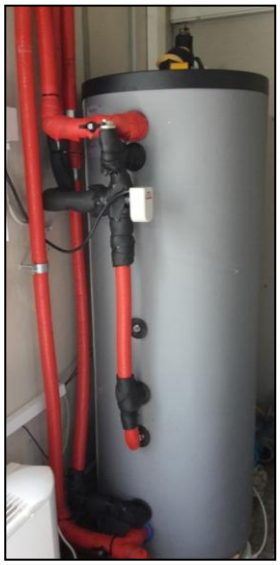

(b) "*intermediate-temperature*" tank

(c) Plate heat exchanger between the heat pump and the "*intermediate-temperature*" tank

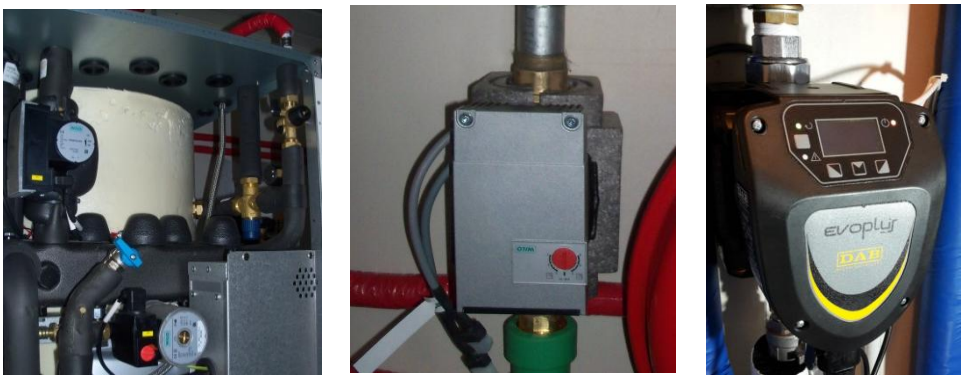

(d) Pumpes employed in the system (from let to right : *P4*, *P2* and *P1*)

Figure 3: Details on the experimental setup

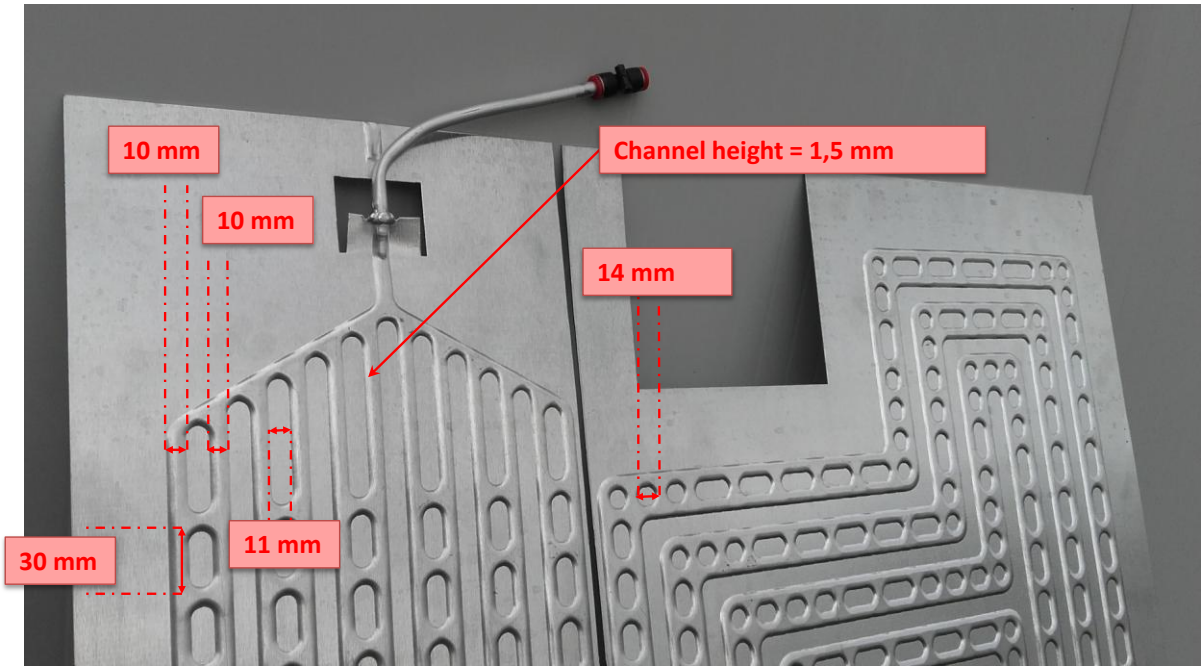

Figure 4: Details of the roll-bond employed in the PVT panels

Table 2. Details the PVT panel - Absorber (Figure 3)

Parameter	Unit	Value
Absorber area	[m^2]	1428
Material	-	Aluminium
Thickness (insulant + absorber)	[mm]	23
Dimensions	[mm x mm]	910x1570
FinWidth	[mm]	15
Fin thickness	[mm]	15
Number of risers	[-]	18
Riser diameter	[mm]	10
Distance between risers	[mm]	10
Internal volume	[l]	0.8

Table 3. Details the PVT panel – Module types and solar cells

Parameter	Unit	Value
Module dimensions	[mm x mm x mm]	1663x998x38
Module area	[m^2]	1.6597
Module weight	[kg]	18
Cell type technology	-	Polycristallinesilicon
Cell manufacturer/model	-	Gintech/GIN156M-3BB
Cell dimensions	[mm]	156x156
Cell thickness	[µm]	200
Cell area	[cm^2]	24.336

2.2 Operation modes and control

This paper reports the results of a monitoring campaign subdivided into four sessions: the first lasted from the 17th of January 2017 until the 13th of March 2017 (heating mode, without *DHW* production), the second lasted from the 13th of March 2017 until the 24th of May 2017 (heating mode, with *DHW* production), the third lasted from the 24th of May 2017 until the 18th of September 2017 (cooling mode, with *DHW* production) and the forth lasted from 22th of October 2017 until the 14th of December 2017. The operation set points were 22°C and 24°C (automatically controlled via a wall-mounted thermostat) in heating and cooling mode, respectively. Each mode was controlled aiming to (a) minimize the electricity consumption by the heat pump, by using solar thermal energy, and (b) maximize the production of electricity of *PVT* panels keeping their operating temperature as low as possible. The detailed operating principles for each mode are provided in the following.

- **Operation mode#1. Heating mode without *DHW* production (from 17/01/2017 to 13/03/2017).** The internal set-point temperature was set to $T_{set\text{-}point}$ = 22 °C, with night attenuation of 4 °C (from 22.00 to 7.00). In this operation mode, the temperature of the water produced by the heat pump and sent to the fan-coils was set by using a climatic curve: T_3 = 45 °C with T_{amb} = 0 °C and T_3 = 40 °C with T_{amb} = 15 °C. In this operation mode, valve *V1* was set to deviate all thermal energy produced by the *PVT* panels to the "*intermediate-temperature*" storage tank. The "*intermediate-temperature*" storage tank, is used as the "*water-source*" for the heat pump when T_{amb}, is low and the resulting *COP* would decrease. Changes from "*air-source*" evaporator to "*water-source*" evaporator are obtained by switching on/off the pump *P2* and switching on/off the outdoor "*air-source*" unit.

- **Operation mode#2. Heating mode with *DHW* production (from 13/03/2017 to 24/05/2017).** The operation mode *mode#1* was modified as follows: (a) a daily profile of *DHW* production was set to produce 1*50 l* (corresponding to, approximately, 4 KWh); (b) valve *V1* was set to deviate the glycol-water mixture, at the outlet of the *PVT* panels, depending on the temperature of the storage tanks (a) towards the "*intermediate-temperature*" storage tank ($T_{intermediate\text{-}temperature}$ < 38 °C), (b) towards the *DHW* tank ($T_{intermediate\text{-}temperature}$ ≥ 38 °C) or towards the "*intermediate-temperature*" storage tank ($T_{DHW,tank}$ ≥ 58 °C); (c) the *DHW* storage tank set-point temperature was set to $T_{DHW,set\text{-}point}$ = 48°C and its lower temperature has been set $T_{DHW,mantenance}$ = 42°C. If the temperature of the *DHW* storage tank fell below $T_{DHW,mantenance}$, the heat pump would be used to increase the *DHW* tank temperature.

- **Operation mode#3. Cooling mode with *DHW* production (from 24/05/2017 to 16/10/2017).** The

internal set-point temperature was set to $T_{set\text{-}point}$ = 24 °C. In addition, the operation mode *mode#2* was modified as follows: (a) a daily profile of *DHW* production was set to produce 1*50 l* (corresponding to approximately, 3 KWh; the DHW corresponding capacity is lower compared with the previous operation mode, owing to the higher inlet water temperature, T_1); (b) valve *V1* was set to deviate the glycol-water mixture, at the outlet of the *PVT* panels, depending on the temperature of the storage tanks towards the *DHW* storage tank ($T_{intermediate\text{-}temperature} \geq$ 36 °C) or towards the "*intermediate-temperature*" storage tank ($T_{DHW,tank} \geq$ 57 °C). In this operation mode, pump *P1* was always activated from 19:00 untill 24:00, in order to lower the temperature of the "*intermediate-temperature*" storage tank and, thus, to increase the *PVT* performances.

- **Operation mode#4. Heating mode without *DHW* production (from 22/10/2017 to 14/12/2017).** The same as Operation mode#1.

Please note that, owing to technical maintenance in the area of the facility, we were forced to stop the monitoring activities in the period between the 16/10/2017 and the 22/10/2017. The outlet water temperature, sent from the heat pump to the fan-coils, was set as follows, depending on the operation mode and the ambient temperature:

- **Operation mode#1, Operation mode#2 and Operation mode#4.** A weather compensation strategy was employed. It means that a controller measures the temperature outside the building and varies the temperature of the water supplied to the heating systems accordingly. The water temperature was set at 45°C if outdoor air temperature was below 0°C, whilst if the outdoor air temperature increased, the outlet water temperature was reduced linearly up to 40°C, if outdoor air temperature was above 15°C
- **Operation mode #3.** The outlet water temperature was set at 7°C;

2.3 Measurement system

All the main variables needed to describe mass and energy balances were measured, as displayed in Figure 5 (please note that Figure 5 provides all details concerning system layout and measured variables). In the following of this section, the main details of the experimental procedure are presented and discussed; conversely, Table 4 summarized main uncertainties of the measurement devices. The flow rate in each circuit was measured by an electromagnetic flowmeter (E&H Promag P50, ±0.2% read value). Evaporating and

condensing pressures were measured by pressure transducers (Keller series 21Y, figure 6a). All the inlet and outlet temperatures of the main equipments, the supply and return water temperatures at the different locations were measured by RTD Pt100 4wire 1/5DIN, inserted inside the pipes (Figure 6b, c and d). In addition, the *PV* and *PVT* back temperatures were measured by RTD Pt100 4wire 1/5DIN. The indoor and outdoor (near the PVT panels) temperature and humidity were measured by an Pt100 4wire hygrometer (Siap+Micros). The solar irradiance was measured by a thermopile pyranometers (Kipp&Zonen CMP11), mounted at a 45° inclined angle near the PVT panels. The power consumption of the heat pump and the circulating pumps (solar pumps, intermediate-storage tank pump, fan-coil pump) were measured by multifunction electric meters (Shark 100 and FRER MonoNano). All the temperature probes were verified with an in-house calibration procedure by using thermostatic bath. All data were recorded automatically every 6 seconds in a data logger (Advantech ADAM 5000 and 4000 data logging devices) to be further post-processed. It is worth noting that all pipes were insulated in order to avoid thermal losses towards the environments (see Figure 6).

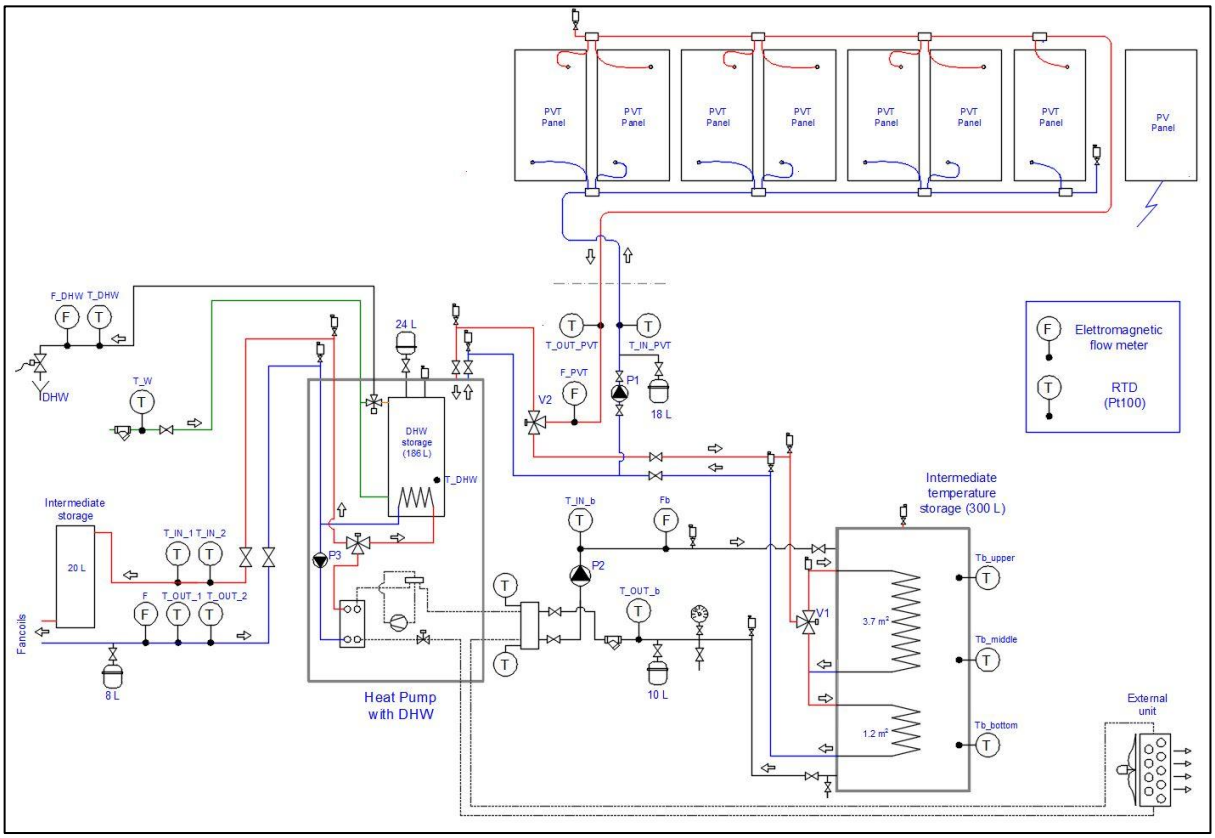

Figure 5: Measurement location

296 **Table 4. Details on experimental uncertainties**

Parameter	Type	Uncertainties
Temperature measurements of water	RTD Pt100 (1/5DIN)	± 0,06°C (at 0°C)
Water volumetric flow rate	Electromagnetic flow meter	± 0,5% read value
Electrical consumption of the heat pump and power	Multifunction power and energy meter	± 0,2% read value
	Transducer	± 0,5% read value
Outdoor air temperature	RTD Pt100 (Class A)	± 0,15°C (at 0°C)
Outdoor relative air humidity	Humidity transmitter	± 1% read value
Indoor air temperature	RTD Pt100 (1/5DIN)	± 0,06°C (at 0°C)

297

(a) Pressure measurement

(b) "intermediate-storage" temperature measurements

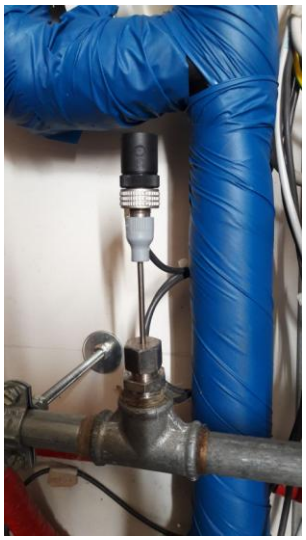

(c) temperature measurements

(d) temperature measurements

298 **Figure 6: Details on the measurement techniques**

2.4 Performance evaluation

2.4.1 Heat pump

The performance of the system was evaluated by means of the mass and energy balances that are evaluated based on the recorded data (flow rates and temperatures). In particular, the energy fluxes across every component were computed as follows:

$$\dot{Q} = \dot{m} c_p (T_{inlet} - T_{outlet}) \quad (1)$$

In Eq. (1), T_{inlet} and T_{outlet} refer to the inlet and outlet temperatures, m is the mass flow rate, c_p is the specific heat of water. From Eq. (1), the corresponding energy can be computed based on the time discretization of the measurements (viz., $E = \sum_{t=0}^{n=N} Q$, where t is the time variable). Based on the heat flow rate and the electric power measured, the *COP* (during heating mode; *mode#1* and *mode#2*, Eq. (2)) and the *EER* (during the cooling mode; *mode#3*, Eq. (3)) were computed as follows:

$$COP = \frac{\dot{Q}_{HP \rightarrow fan-coil} + \dot{Q}_{HP \rightarrow DHW-tank}}{P_{el}} \quad (2)$$

$$EER = \frac{\dot{Q}_{HP \leftarrow fan-coil} + \dot{Q}_{HP \rightarrow DHW-tank}}{P_{el}} \quad (3)$$

In Eqs. (2-3), P_{el} is the electric power provided to the systems; $\dot{Q}_{HP \rightarrow fan-coil}$ and $\dot{Q}_{HP \leftarrow fan-coil}$ is computed based on T_3 and T_4 and $\dot{m}_3 = \dot{m}_4$ (please refer to Figure 1 for the location of the subscripts) and refer to the heat transfer from the heat pump towards the fan-coils and vice-versa; conversely, $\dot{Q}_{HP \rightarrow DHW-tank}$ refers to the heat flow rate provided by the heat pump to the *DHW* tank and is computed as follows:

$$\dot{Q}_{HP \rightarrow DHW-tank} = \frac{\rho V_{DHW,tank} c_p (T_{t=n} - T_{t=n-1})}{\Delta t_{sampling}} \quad (4)$$

In Eq. (4), $V_{DHW,tank}$ is the volume of the *DHW* tank, ρ is the density of water, and t is the time variable. Please note that Eq. (4) is computed under the following constrains: (a) the temperature of the *DHW* boiler is below $T_{DHW,maintenance}$, (b) the temperature of the *DHW* storage tank is increasing with time; (c) heat pump status is ON; (d) perfect mixing within the storage tank is assumed. From Eq. (4), the corresponding energy can be computed based on the time discretization of the measurements (viz., $E = \sum_{t=0}^{n=N} Q$, where t is the time variable).

To study the influence of the "*water source*" evaporator and the "*air-source*" evaporator, Eq. (2) was modified as follows, based on the status of the storage tank circulating pump (pump *P2*, Figure 1):

$$COP_{"water\text{-}source"} = \frac{\dot{Q}_{HP \rightarrow fan-coil} + \dot{Q}_{HP \rightarrow DHW-tank}}{P_{el}} \quad if\ pump\ P2 = ON \tag{5}$$

$$COP_{"air\text{-}source"} = \frac{\dot{Q}_{HP \rightarrow fan-coil} + \dot{Q}_{HP \rightarrow DHW-tank}}{P_{el}} \quad if\ pump\ P2 = OFF \tag{6}$$

Based on experimental uncertainties, it is estimated that the COP/EER is computed within the range of ± 0.2 % of its actual value. It is worth noting that, when not explicitly stated, the heat pump consumptions include also all the auxiliaries: (a) the solar circulating pump (its consumption was approximately 4.1 % of the total energy consumption); (b) the "*intermediate-temperature*" circulating pump (its consumption was approximately 1.2 % of the total energy consumption); (c) the Fan-coil circulating pump (its consumption was approximately 3.7 % of the total energy consumption), (d) the DHW circulating pump and all other auxiliaries (their consumptions were approximately 14.2 % of the total energy consumption). The above-mentioned values consider all days in the monitored period.

Finally, it is worth nothing that, in the operation *mode#3*, the glycol-water mixture, at the outlet of the *PVT* panels, can be deviated towards the *DHW* storage tank, to reduce the heat pump energy consumption for the DHW production (please refer to Section 2.2). In particular, the heat provided by the PVT panels to the *DHW* tank, $Q_{PVT \rightarrow DHW\text{-}tank}$, is computed as follows:

$$Q_{PVT \rightarrow DHW-tank} = \frac{\rho V_{DHW,tank} c_p (T_{t=n} - T_{t=n-1})}{\Delta t_{sampling}} \tag{7}$$

Please note that Eq. (7) is computed under the following constrains (please refer to Section 2.2 for further details on this operation mode): (a) $T_{intermediate\text{-}temperature} \geq 36$ °C, (c) $T_{DHW,tank} < 57$ °C, (c) the temperature of the *DHW* storage tank is increasing with time; (c) pump *P1* status is ON.

2.4.2 PVT panels

The electrical and thermal efficiency of the PVT panels is computed as follows:

$$\eta_{el} = \frac{P_{el,PVT}}{\int_0^{t_{final}} A_{PVT} G d\tau} \tag{8}$$

$$\eta_{th} = \frac{P_{th,PVT}}{\int_0^{t_{final}} A_{PVT} G d\tau} \tag{9}$$

Where *A* is the total area of the panels. Similarly, the electrical efficiency of the PV panel is computed as follows:

$$\eta_{el} = \frac{P_{el,PV}}{\int_0^{t_{final}} A_{PV} G d\tau} \quad (10)$$

The reader should refer to the many review presented in the literature for further details on the relationships between these efficiencies and operating conditions of the panels (see, for example, ref. [21]).

3 Experimental results

In this section, the experimental results are presented and discussed. First, the ambient conditions in the monitored period (viz. ambient temperature and humidity) are presented. Second, the seasonal time-scale performance and the daily time-scale performance of the systems are discussed. In particular, the influence of the "*water-source*" and the "*air-source*" evaporators on the heat pump performances are analysed.

3.1 Ambient conditions

Figure 7 displays the ambient conditions in the monitored period, in order to provide an overview of the heat pump working conditions and boundary conditions. In particular, Figure 7 displays the daily-averaged values of the ambient temperature (T_{amb}) and relative humidity, which is an important parameter for heating demand in summer, and frost issue in winter, see ref. [11]. The heat pump was operated in a quite broad range of operating conditions (i.e., daily averaged T_{amb} ranged between 0 and 33 °C; conversely, the instantaneous values of T_{amb} , which are not presented here, ranged between -5°C and 40 °C).

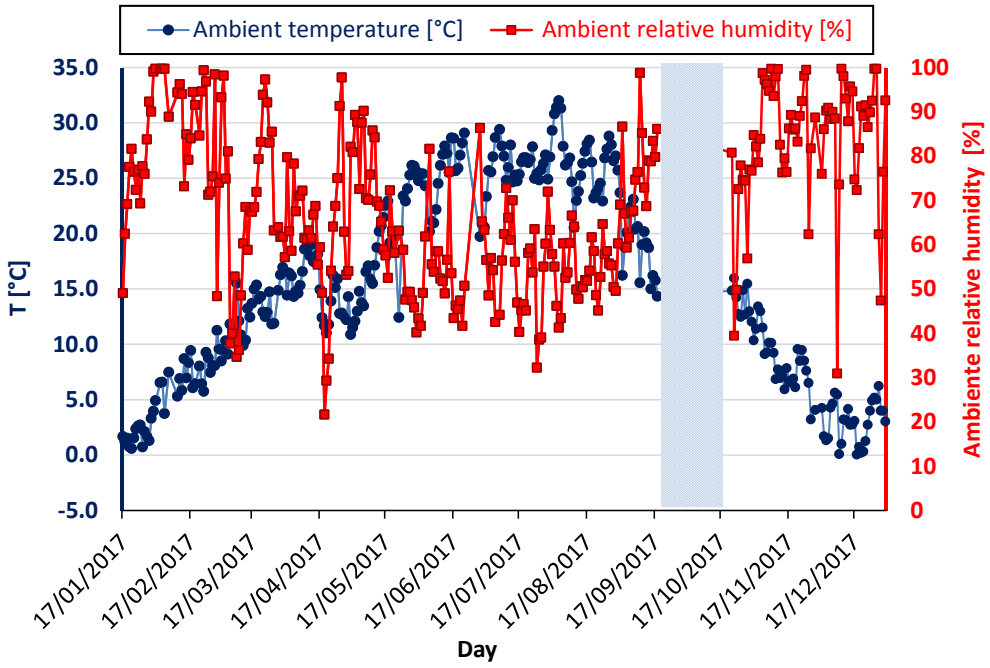

Figure 7: Daily-averaged ambient conditions: ambient temperature and relative humidity

3.2 Seasonal performance

3.2.1 Analysis of the seasonal performances

Figure 8 displays the daily-averaged performance of the multifunctional heat pump in the four operating modes, listed and described in Section 2.2. Please note that, in Figure 8, T_{amb} is also displayed for the sake of clarity. In addition, Table 5 and Table 6 display the monthly-averaged and operation mode-averaged performance of the system, respectively. The performance of the multifunctional heat pump was computed by using Eq. (2)—the *COP*—and Eq. (3)—the *EER*. In the operation *mode#1*, the useful effect of the heat pump is $Q_{HP \rightarrow fan\text{-}coil}$ (there is no *DHW* production; $Q_{HP \rightarrow DWH\text{-}tank}$ = 0); conversely, in the other operation modes (viz. operation *mode#2* and *mode#3*) the useful effect of the heat pump consists in both $Q_{HP \rightarrow fan\text{-}coil}$ and $Q_{HP \rightarrow DWH\text{-}tank}$. Please note that, in Figure 8, the electric consumption, P_{el}, used in input to evaluate *COP* and *EER* does not account for the contribution of the auxiliaries (i.e., circulation pumps, stand-by consumption, and so on …), as discussed in Section 2.3. The influence of auxiliaries on electrical consumption (and, thus, the performance of the systems), have been commented in Section 2.3 and are displayed in Figure 9. It is worth noting that the electrical consumption of the system is strongly related to the external ambient conditions and internal temperature set-point owing to the well-known relations between external temperature, internal temperature and heat pump load. Therefore, the shape of the electrical consumption (Figure 9) is, somehow, specular to the shape of T_{amb} (Figure 7).

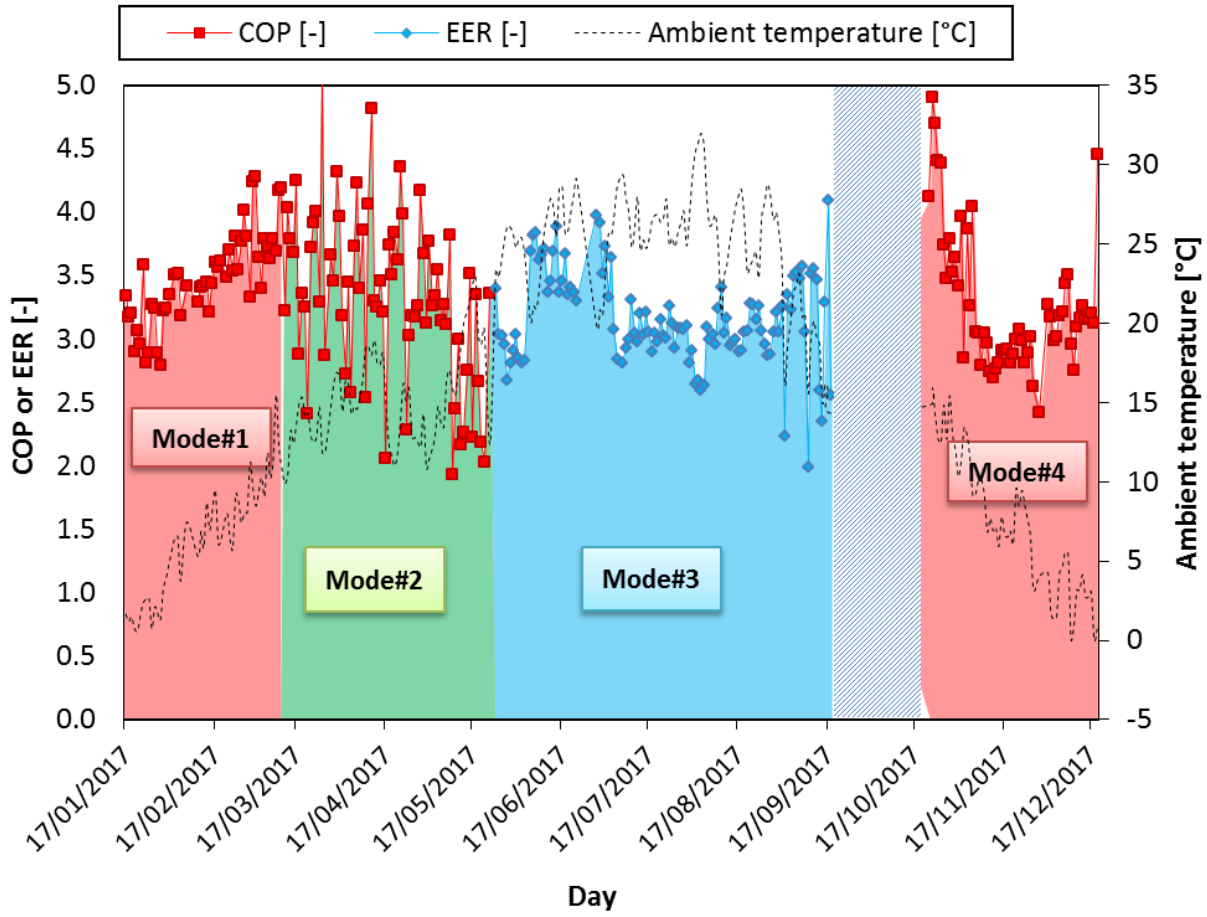

373

374 **Figure 8: Daily-averaged performance of the multifunctional heat pump depending on the operation mode**

375 **and ambient temperature**

376 **Table 5. Monthly-averaged performances (auxiliaries are neglected when presenting $En_{el,PdC}$)**

Month	Operation mode	$En_{th,fan\text{-}coil}$ [kWh]	$En_{th,DHW}$ [kWh]	$En_{el,PdC}$ [kWh]	COP [-]	EER [-]
January	mode#1	646.7	-	210.3	3.08	-
February	mode#1	670.4	-	191.1	3.51	-
March	mode#1	202.6	-	54.0	3.75	-
March	mode#2	151.3	89.3	87.8	2.74	-
April	mode#2	136.1	151.2	116.4	2.47	-
May	mode#2	75.9	103.6	70.3	2.55	-
May	mode#3	137.7	31.6	56.6	-	2.99
June	mode#3	802.6	92.4	259.7	-	3.45
July	mode#3	1226.5	111.9	429.1	-	3.12
August	mode#3	1316.0	109.4	471.5	-	3.02
September	mode#3	310.5	67.2	123.4	-	3.06
October	mode#4	69.4	-	19.6	3.53	-
November	mode#4	583.2	-	209.4	2.78	-
December	mode#4	944.1	-	309.7	3.05	-

377

Table 6. Operation mode-averaged performances (auxiliaries are neglected)

Operation mode	$En_{th,fan\text{-}coil}$ [kWh]	$En_{th,DHW}$ [kWh]	$En_{el,PdC}$ [kWh]	COP [-]	EER [-]
mode#1	1519.6	0.0	455.4	3.34	-
mode#2	363.2	344.2	274.5	2.58	-
mode#3	3793.3	412.5	1340.4	-	3.14
mode#4	1617.0	6.0	547.3	2.97	-

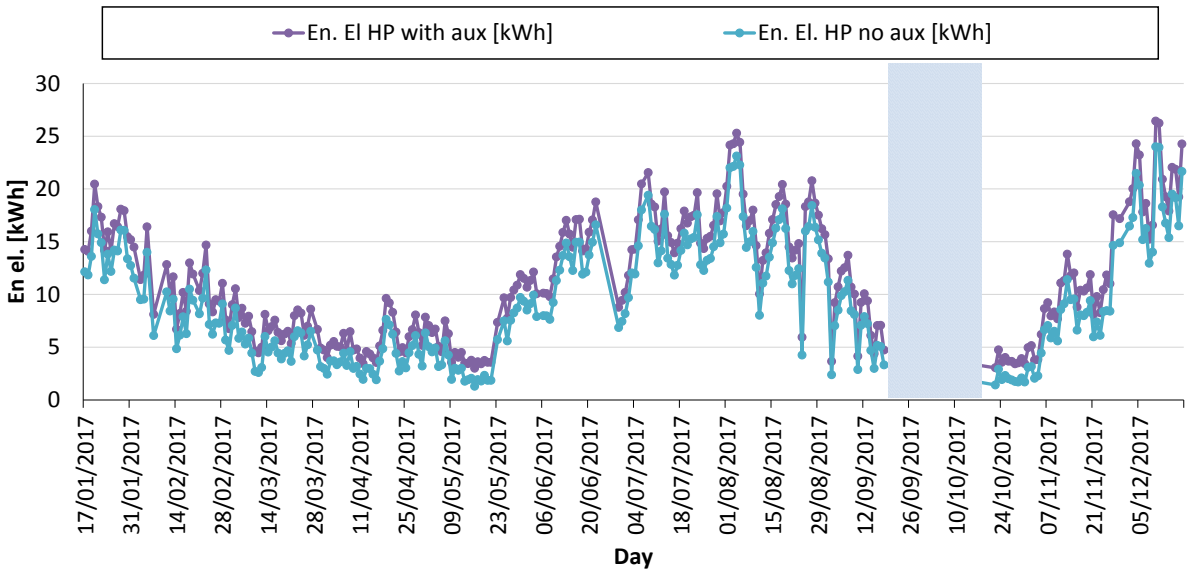

Figure 9: Influence of auxiliaries on electrical consumption of the systems - Refer to figure 8 for details on the operation mode

Now, further details on the three different operation modes are discussed; in this respect, aside from the above-mentioned figures. In the operation mode *mode#1*, the monthly-averaged *COP* is in the range of 3 and 4.5 (Table 5) and the averaged COP value is equal to 3.34 (Table 6); as expected, *COP* increases with time, owing to the increasing daily-averaged T_{amb} (Figure 7 and Figure 8). The relationship between T_{amb} and the heat pump performance can be further understood, by considering the layout of the system. Indeed, the performance of an heat pump may be related (for fixed component design), to the evaporating and condensing temperatures/pressures. In the present case: (a) the condensing pressure is related to the internal ambient conditions, that, for a fixed set-point are, approximately, periodical with time; (b) evaporating temperature T_{eva} is related to T_{amb}, owing to the variable speed compressor and the electronic expansion valve (see the details in Section 2.1). Therefore, a variation in the ambient temperature, mainly affects T_{eva} and, thus, affects the performance of the whole system. To better discuss this concept, Figure 10 displays the relationship between the variables of the heat pump (i.e., evaporator pressure and condensing pressure), T_{eva} and *COP*. The reader may refer to the studies proposed by Kuang and Wang [38] and Ma and Zhao [39] for a

more detailed discussion on the role of variable speed compressors in heat pumps. In addition, in Figure 10 is also displayed the influence of the "*water-source*" evaporator. The influence of the "*water-source*" evaporator is further discussed in Section 3.3.

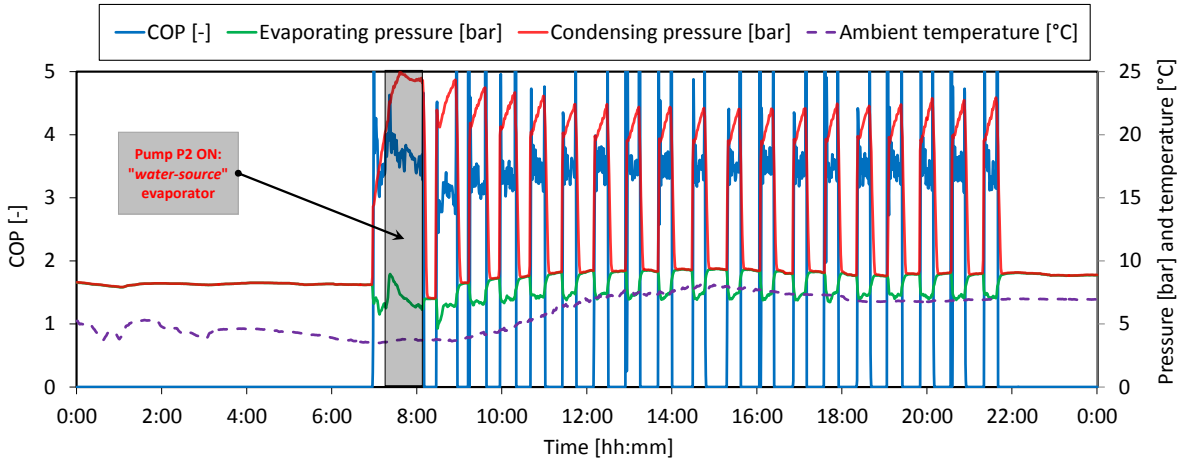

Figure 10: Daily performance of the multifunctional heat pump: performance parameters (data obtained at 13/02/2017, *mode#1*)

In the operation mode *mode#2* the performance of the system, compared with the one observed in *mode#1*, shows a larger variability and *COP* is slightly lower. The monthly-averaged *COP* is in the range of 2.0 and 4.5 (Table 5) and the averaged *COP* value is equal to 2.58 (Table 6). This behavior can be explained based on the system operations as well as on the ambient conditions. First, in this period, beside DHW production, $Q_{HP \rightarrow fan\text{-}coil}$ is very low and, in some days, $Q_{HP \rightarrow fan\text{-}coil} \approx 0$, owing to the high T_{amb} (the internal set-point temperature can be achieved also with very low heat pump load). This consideration is also displayed in the heat fluxes reported in Figure 11, where it is shown that the thermal flux of the fan-coils from/towards the internal ambient is very low. Therefore, *COP* is mostly related to $Q_{DHW\text{-}tank}$. Second, it should be noted that $Q_{HP \rightarrow DHW\text{-}tank}$ is produced at higher temperature compared with $Q_{HP \rightarrow fan\text{-}coil}$; therefore the expected performance of the heat pump is reduced. In this respect it is well known that Eq. (2) does not take into account the grade of heat produced, as it is related to energy balances and neglect the entropy/exergy concept. In the operation mode *mode#3*, in the cooling mode with DHW production, the monthly-averaged *EER* is in the range of 3 and 4.5 (Table 5) and the averaged *EER* value is equal to 3.14 (Table 6). The discussion concerning the relationship between the ambient conditions and the system performance is similar to the above-discussion for the operation mode *mode#1*. It is worth noting that, owing to the high ambient temperature, in the summer season, the *PVT* panels are able to contribute to the maintenance temperature of the *DHW* storage tank, thus

reducing $Q_{HP \rightarrow DHW\text{-}tank}$ and, thus, the overall energy consumption of the heat pump. In this respect, Table 7 summarize the energy fluxes provided either by the heat pump or by the *PVT* panels to the *DHW* storage tank. It is observed that thermal energy produced by the PVT panels have been successfully used to support the production of DHW in the summer season; in particular, approximately 63% of the heat needed by the DHW storage tank has been ensured by the PVT panels (the remaining has been produced by the heat pump).

Table 7. Contribution provided by the PVT panels to the DHW storage tank

	$En_{HP \rightarrow DHW\text{-}tank}$* [kWh]	$En_{PVT \rightarrow DHW\text{-}tank}$** [kWh]	*Contribution provided by the PVT panels*** [%]
May	28.15	46.89	62.49%
June	90.96	156.23	63.20%
July	86.08	178.85	67.51%
August	75.42	197.98	72.41%
September	91.21	56.71	38.34%
Total	371.82	636.66	63.13%

* Computed by integrating Eq. (4) over the months

** Computed by integrating Eq. (7) over the months

*** Computed by $100 * \frac{Q_{PVT \rightarrow DHW-tank}}{(Q_{DWH \rightarrow DHW-tank} + Q_{PVT \rightarrow DHW-tank})}$

Finally, in the operation mode *mode#4*, the monthly-averaged *COP* is in the range of 3 and 4.5 (Table 5) and the averaged COP value is equal to 2.97 (Table 6); as the operating conditions of operation mode#4 are equal to the ones in operation mode#1, the same comments as above, also apply here. For the sake of clarity, Figure 11 displays the input-output energy fluxes considering the heat pump as control volume. The electrical consumption of the heat pump reflects the ambient conditions, as stated above. It is worth noting that, in the summer period, the thermal energy produced by the PVT panels have been successfully used to support the production of *DHW*.

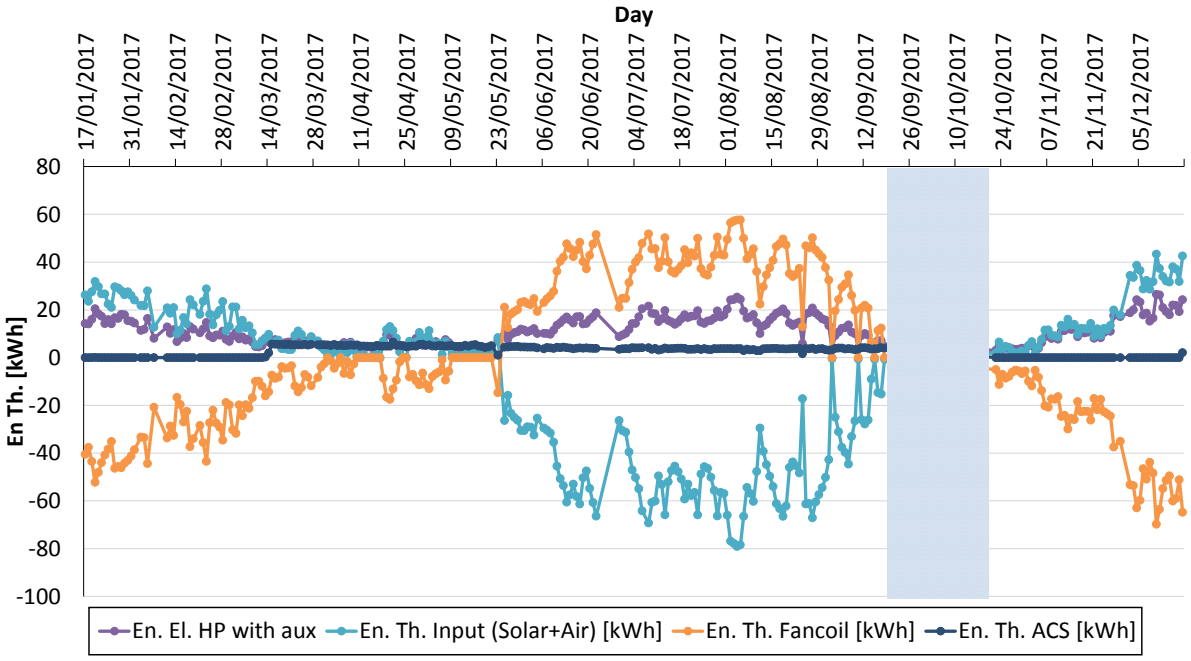

Figure 11: Thermal energy fluxes - Refer to Figure 8 for details on the operation mode

3.2.2 Comparison between water source and air source

In the previous section, the performances of the whole system was discussed, without any reference to the heat source used by the multifunctional heat pump. In this section, an insight in the performance of the system is proposed, by analyzing the contribution of the "*water-source*" evaporator and the "*air-source*" evaporator to achieve the averaged performance described in Section 3.2.1. To this end, by applying Eqs. (5-6) in the in the operation mode *mode#1* and operation *mode#4*, the corresponding "*water-source*" the "*air-source*" performances were obtained; the results of this analysis were summarized in Figure 12, in terms of daily-averaged values and in Table 8, in terms of monthly-averaged values. Please note that in some days (viz. the data not displayed in Figure 12), the "*water-source*" evaporator was not used. Applying the whole dataset, (in the operation mode#1) and applying Eqs. (5-6), an average *COP* increase approximately 34 % from the "*air-source*" mode to the "*water-source*" mode was observed (please refer to Table 8 for the details concerning the performance parameters).

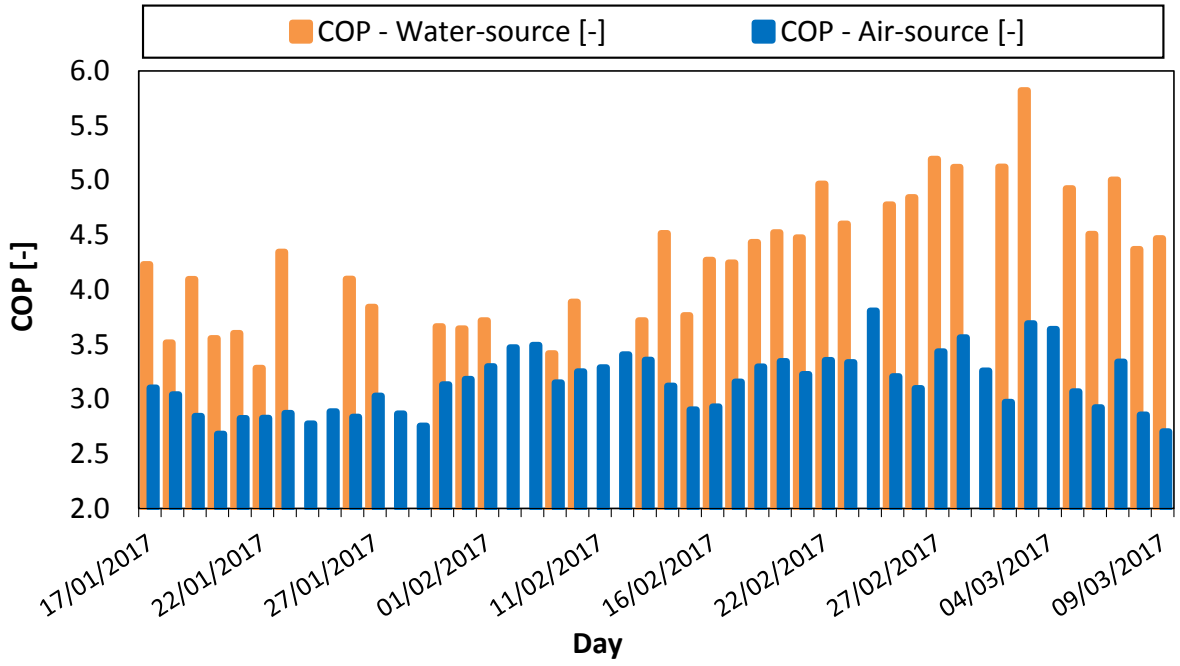

(a) data obtained during operation *mode#1*

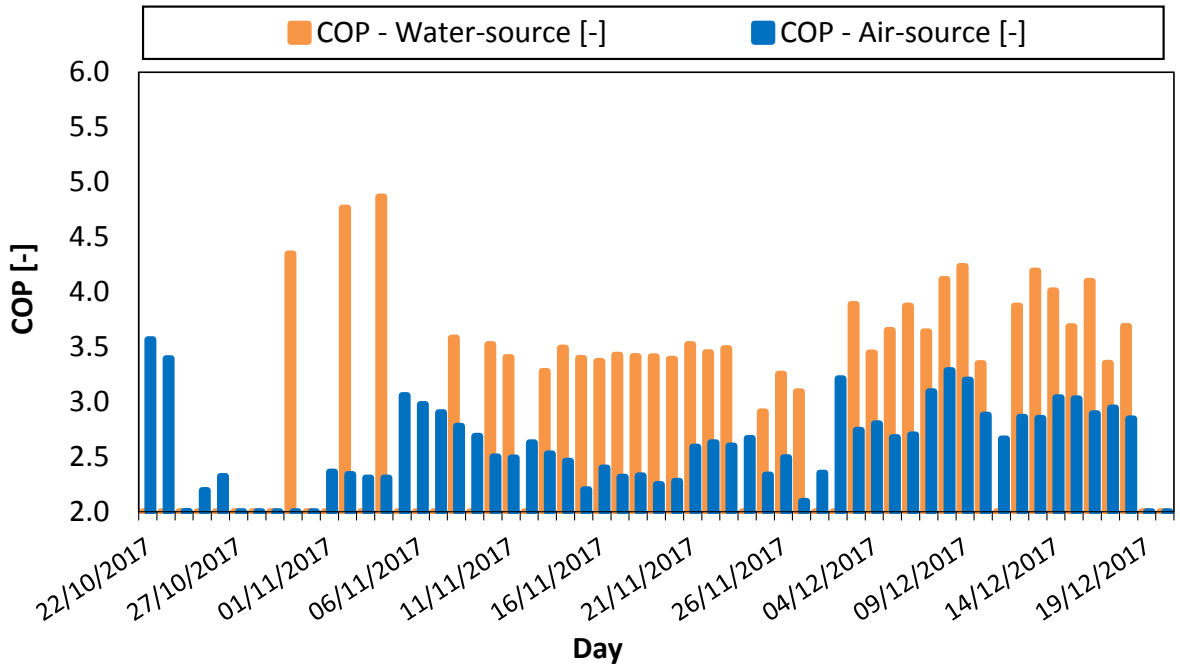

(b) data obtained during operation *mode#4*

447 **Figure 12: Daily-averaged performance of the multifunctional heat pump: influence of "*water-source*" and**
448 **"*air-source*" evaporators (operation mode *mode#1* and operation *mode#4*)**

449 It is also observed that, when the "*water-source*" evaporator was used, defrost of the heat pump has been
450 avoided; indeed, the "*water-source*" evaporator has been operated mainly in the coolest hors of the day: the
451 reader should refer to Section 3.3.1 and Section 3.3.2 for a better description of the daily system performance,

based on the hourly profiles of the variables. Defrosts was observed in three days only, when the "*water-source*" evaporator was not available (owing to the low temperature of the "*intermediate-storage*"). The corresponding energy consumption of the defrosts is approximately 0.1 kWh. Therefore, it is reasonable to state that the application of the *water-source*" evaporator not only increased the *COP*, owing to an higher heat source (See Section 3.3.2), but also avoided additional energy consumption.

Table 8. Comparison between "*water-source*" and "*air-source*" evaporators (auxiliaries are neglected)

	$En_{th,fan-coil}$ "*water-source*" [kWh]	$En_{th,fan-coil}$ - "*air-source*" [kWh]	$En_{el,PdC}$ - "*water-source*" [kWh]	$En_{el,PdC}$ - "*air-source*" [kWh]	COP "*water-source*" [-]	COP "*air-source*" [-]	COP Averaged [-]	ΔCOP "*water-source*" and "*air-source*" [%]
January	155.18	491.53	40.58	169.69	3.82	2.90	3.08	32.03%
February	144.79	525.59	32.79	158.30	4.42	3.32	3.51	32.98%
March	78.62	123.94	16.36	37.64	4.81	3.29	3.75	46.00%
October	40.82	28.56	7.76	11.89	5.26	2.40	3.53	118.85%
November	216.57	366.61	63.26	146.17	3.42	2.51	2.78	36.49%
December	193.01	750.03	51.40	257.79	3.76	2.91	3.05	29.08%
Total	828.99	2286.25	212.15	781.48	3.91	2.93	3.14	33.6%

3.2.3 Comparison between PV and PVT panels

In this section, the performance of the PV and PVT panels are compared in terms of efficiencies and energy production. To this end, Figures 13 - 17 summarize the main outcomes of the field trial from the seasonal point of view. The reader should refer to Section 3.3.3 for a better description of the daily performances. Figure 13 compares the cell temperatures ($T_{cell,PVT}$ *and* $T_{cell,PV}$) and electrical efficiency of the PVT (Eq. (8)) and PV (Eq. (10)) panels. In particular, Figure 13a displays the daily-averaged variables and Figure 13b displays the values of the variables averaged in the period between 10:00 and 16:00, to take into account only of the periods of the day when *PV* and *PVT* panels are producing thermal/electrical energy. Please note that the *PVT* cell temperatures were not monitored up to the 10th of February 2017, which is the reason of its value equal to 0 in Figure 13a and Figure 13b. It is observed that the cell temperature are highly related to T_{amb} (Figure 7); thus, it is not surprisingly that the shape of T_{cell} profile is somehow similar to the shape of T_{amb} profile. The electrical efficiency of the panels and related to the cell temperatures and the ambient conditions, owing to the well-known relationships between temperature and *PV* efficiency (see, for example ref. [40]). Hence, it is not surprisingly that an higher efficiency is observed during the winter period and it slightly decreases with time (owing to the increasing ambient temperatures).

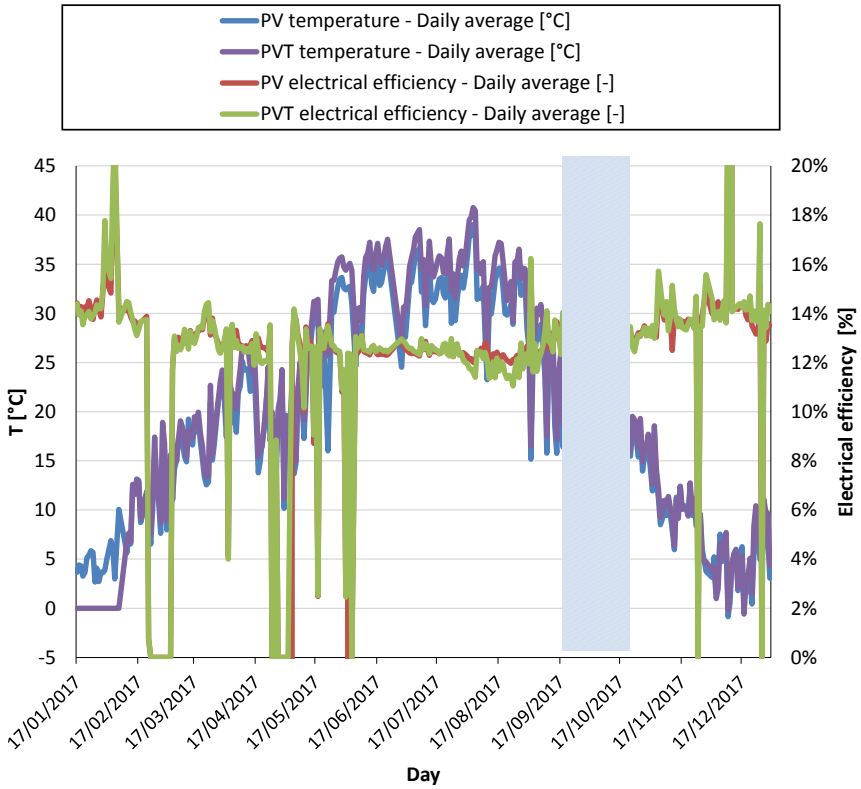

(a) daily-averaged values

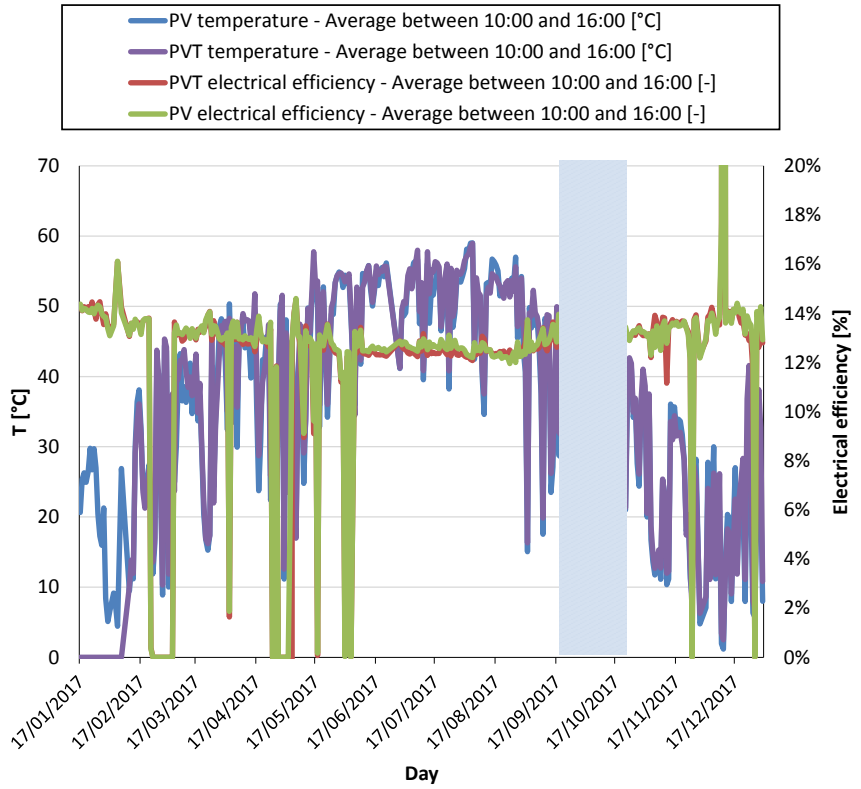

(b) averaged values between 10 and 16

473 **Figure 13. Electrical efficiency and operating conditions of *PVT* and *PV* panels - Refer to Figure 8 for details**

474 **on the operation mode**

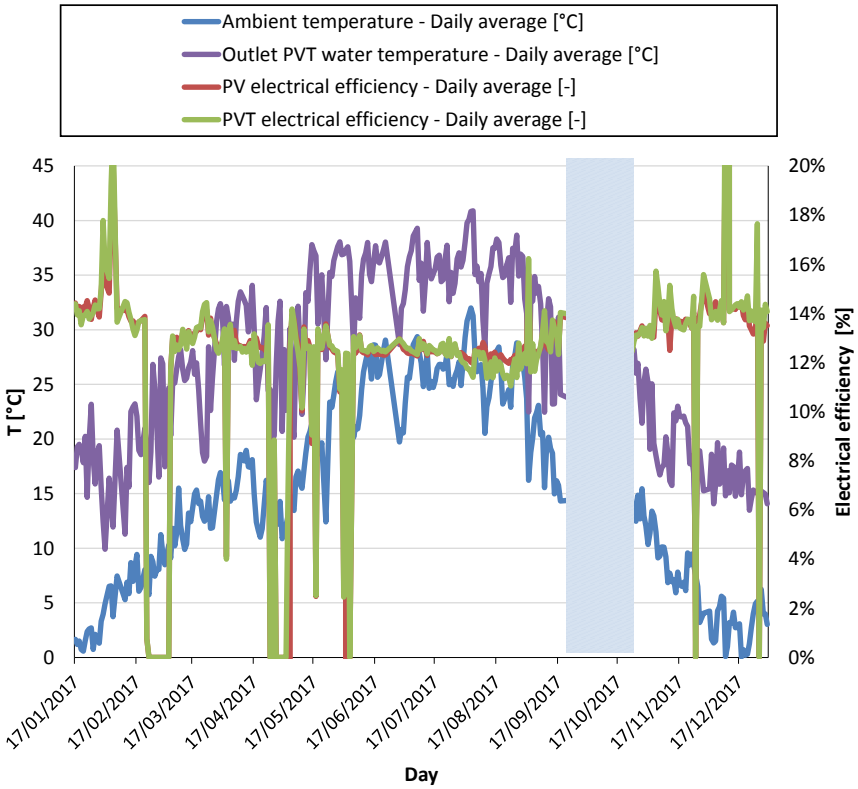

475

476 **Figure 14. Performance and operating conditions of PVT and PV panels - Refer to Figure 8 for details on the**

477 **operation mode**

478 It is worth noting that, in operation *mode#3*, pump *P1* was activated from 19:00 untill 24:00, in order to lower

479 the temperature of the "*intermediate-temperature*" storage tank panels and, thus, to increase the *PVT*

480 performances. It is worth noting that $T_{cell,PVT}$ is generally lower compared with $T_{cell,PV}$, owing to the heat transfer

481 between the panel and the water. Figure 14 contributes and support the previous discussion proposed, by

482 including the relationship between (a) the electrical efficiency, (b) the water temperature at the outler of the

483 PVT panel, (c) $T_{cell,PVT}$ and (d) T_{amb}. It is interesting to observe that the PV electrical efficiency is similar to the

484 PVT electrical efficiency (Figure 13). This point is also clearly observed in Figure 15, where the electrical energy

485 produced per unit area by the PVT and PV panels are compared (energy produced per unit area are used to

486 compare the performance of the seven PVT panels with the performance of a PV panels): the energies (per

487 unit area) produced by the PV and PVT panels are comparable. It can be concluded that, on a seasonal point of

488 view the *PVT* panels are very interesting, being able to produce both electrical and thermal energy, with a

489 comparable energy efficiency.

490 Figure 16 and figure 17 display the thermal production of the PVT panels. Figure 16 displays the relationship

between the thermal efficiency and the cell temperature. The thermal production is highly related to the ambient conditions (Figure 7) and the thermal efficiency ranges between 5% and 30% depending on the ambient and operating conditions. Figure 17 displays the thermal energies produced by the PVT panels. In particular, Figure 17 displays (a) the thermal energy transferred from the PVT panels toward the to the water (positive contribution, Figure 16) and (b) the thermal energy transferred from the water toward the PVT panels (negative contribution, Figure 16). The latter contribution can be interpreted as a thermal loss, but it is employed, in operation mode#3, to decrease the "*intermediate-temperature*" storage tank (by activating pump P1 from 19:00 to 24:00) and, thus, to increase the *PVT* electrical efficiency during the subsequent day.

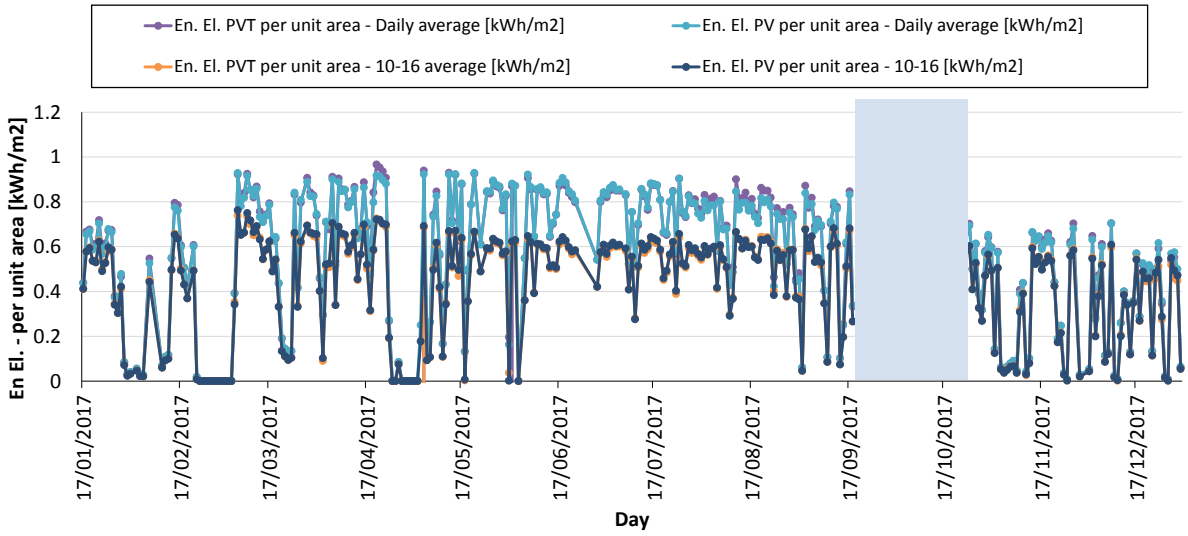

Figure 15. Electrical energy per unit area produced by the PVT and PV panels – Please note that the electrical production is normalized per unit area, to compare the production of the seven *PVT* panels with the performance of a *PV* panels - Refer to Figure 8 for details on the operation mode

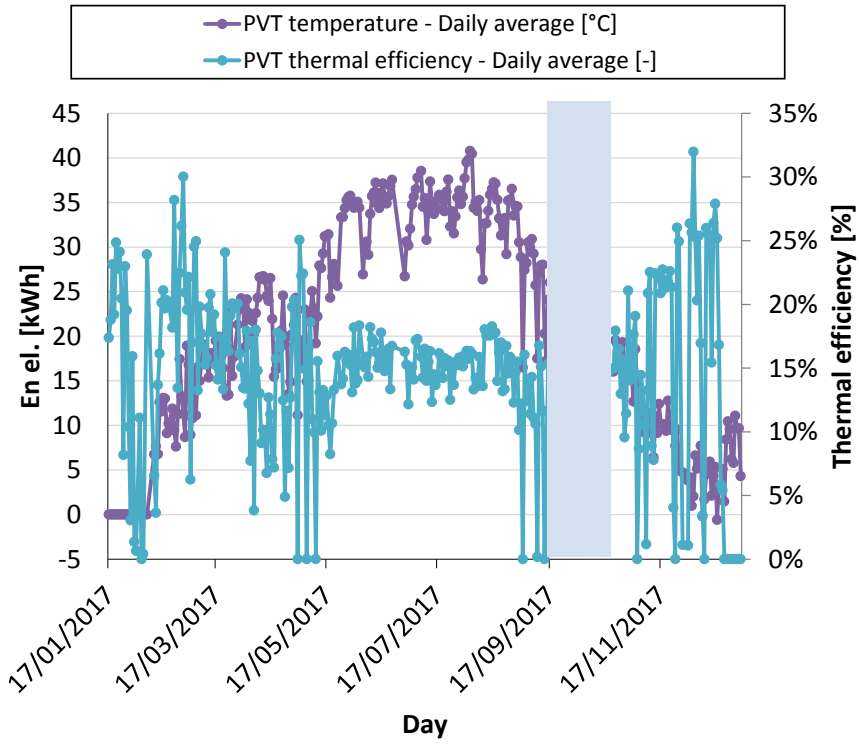

503

504 **Figure 16. Thermal efficiency and operating conditions of *PVT* panels - Refer to Figure 8 for details on the**

505 **operation mode**

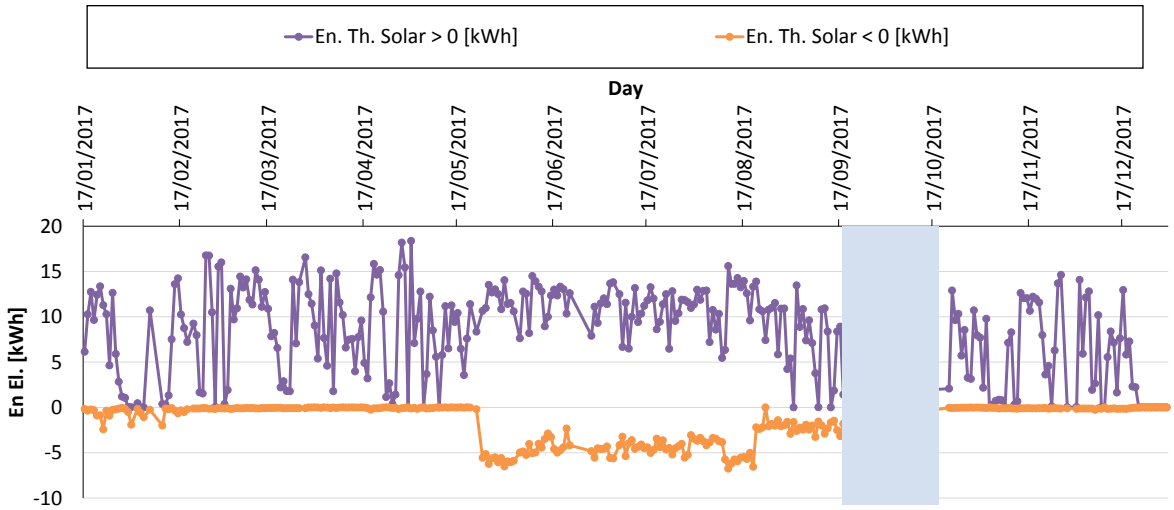

506

507 **Figure 17: Thermal energy fluxes on the PVT panels - Refer to Figure 8 for details on the operation mode**

508 ## 3.3 Daily performance

509 In the previous section (Section 3.2), the seasonal performances of the multifunctional heat pump have been

510 described and commented, in terms of daily-averaged parameters. These parameters provide an overview

concerning the average performance of the system and are related to the instantaneous values of the operating parameters (i.e., temperatures, mass flow rate and pressures). The role of this section is to provide insights on the multifunctional heat pump daily-averaged performance, by discussing the relationships between the instantaneous variables characterizing the system (viz. the variables listed in Section 2.3 and displayed in Figure 5). In order to comment on the instantaneous values of the experimental data, it should be noted that the numerous parameters of the system are highly connected each other, owing to the system configuration (see the layout in Figure 1 and Figure 5); indeed, the multifunctional heat pump is connected to: (a) the *DHW* storage tank (refer to Section 2.2 for the details concerning the *DHW* storage tank temperature set-points); (b) the water-loop which connects the multifunctional heat pump to the external "*air-source*" evaporator and to the "*intermediate-temperature*" storage tank (And, thus, to the solar part of the system); (c) the water-loop which connects the multifunctional heat pump to the fan-coils.

3.3.1 Analysis of the daily performances

In this section, the relationships between the different variables of the systems are described and commented to better discuss the results presented in Section 3.2.1. In particular, Figures 18-24 display the instantaneous values of the measured variables for the three operating modes (for every operation mode, a representative day has been selected):

- operation *mode#1* (heating mode without *DHW* production): experimental data presented in Figures 18, Figure 19 and Figure 26a (data obtained at 13/02/2017);
- operation *mode#2* (heating mode with *DHW* production): experimental data presented in Figures 20, Figure 21 and Figure 26b (data obtained at 17/03/2017);
- operation *mode#3* (cooling mode with *DHW* production): experimental data presented in Figures 22, Figure 23 and Figure 26c (data obtained at 17/07/2017);
- operation *mode#4* (heating mode without *DHW* production): experimental data presented in Figures 24 and Figure 25 (data obtained at 13/02/2017);

As previously mentioned, the instantaneous values of the measured variables are related one-another; for this reason, in the following of this section, a "*bottom-up*" approach (viz. starting from the heat pump itself towards the other systems) is used to present the results: (a) first, the heat pump performance parameters are

commented (Figure 18a, Figure 20a and Figure 22a); (b) second, the relationships between the heat pump performances and boundary conditions (i.e., T_{amb}, "*intermediate-boiler*" temperature, PVT panels temperature and operating conditions, …) are commented (Figure 18b, Figure 20b and Figure 22b); (c) finally, the operating conditions of the other components (i.e., *PVT* panels, "*intermediate-temperature*" storage tank, *DHW* storage tank, …) are presented and commented (Figure 18c, Figure 20c and Figure 22c, and Figure 19 - 24).

Figure 18a, Figure 20a and 22a display the relationships between the control parameters (viz. the status of pump *P1* and pump *P2*) and the performance parameters (viz. either *COP* or *EER*); in addition, in these figures, the influence of auxiliaries on instantaneous system performance are displayed. Please note that in Figure 18a, Figure 20a and Figure 22a, the performance parameters have been computed by neglecting the contribution of $Q_{HP \rightarrow DHW-tank}$, to focus on the heat pump only. In order to better interpret these data, the experimental profiles presented in Figure 10 should be taken into account as well; in Figure 10 it was shown that a variation in T_{amb}, mainly affects T_{eva} and, thus, affects the performance of the whole system, owing to the variable speed compressor and the electronic expansion valve. Hence, based on the instantaneous experimental data (Figure 18a, Figure 20a and Figure 22a) as well as the above-mentioned consideration, three main outcomes can be drawn: (a) the influence of auxiliaries on electrical consumption (and, thus, the performances of the systems) are in agreement with the considerations reported in Section 2.3 and the seasonal time-scale results presented in Figure 9; (b) when the system employs the "*water-source*" evaporator, the performance of the system increases (please refer to Section 3.2.3 and Section 3.3.2 for a more detailed discussion concerning this point); (c) the variations in the performance parameters of the multifunctional heat pump are related to the system boundary conditions (both heat source and heat sink); i.e., the shape of the performance parameter profile reflects the ambient conditions.

Figure 18b, Figure 20b and Figure 22b display the relationships between the instantaneous heat pump performances (in term of *COP*, without taking into account the auxiliaries) and the heat pump boundary conditions (i.e., T_{amb}, the temperature of the "*intermediate-temperature*" storage tank—$T_{\text{"intermediate-temperature" storage tank}}$—, the temperature of the *PVT* panels, the operating conditions of the *PVT* panels …). Considering these instantaneous experimental data, the limited availability of the "*water-source*" evaporator (mentioned in Section 3.2.2 and visualized in Figure 18a and Figure 20a) can be explained. Indeed, the temperature of the "*intermediate-temperature*" storage tank is used as heat source of the heat pump when $T_7 \approx T_{\text{"intermediate-temperature" storage tank}} > T_{amb}$ (please refer to Figure 1 for the locations indicated by the subscripts). This issue was

clearly observed in the early hours in the morning (i.e., approximately between 7:15 and 8:00) in Figure 18b and in Figure 20b: in the early hours in the morning the heat pump starts to restore the internal temperature set point (after the night attenuation, Section 2.2); in this condition, the "*water-source*" is employed, owing to the unfavorable ambient condition and $T_{\text{"intermediate-temperature" storage tank}}$ starts increasing again (see the values of T_7 and T_8), owing to the heat provided by the *PVT* panels (pump *P1* is activated, as can be observed comparing the experimental profiles of Figure 18a, Figure 20a and Figure 18b and Figure 20b). A further insight in the availability of the "*water-source*" is provided in Figure 26, which displays the temperature measurements on the "*intermediate-temperature*" storage tank in different locations (i.e., in the lower section, in the middle section and in the higher section, see Figure 5 and Figure 6b): from these measurements can be observed a certain thermal stratification in the storage tank, which should be considered in future modeling approaches. In addition, the experimental data in Figure 26 support that the availability of the "*water-source*" is related to the "*intermediate-temperature*" storage tank conditions (viz. the temperature); generally, pump *P2* is activated during the morning (when T_{amb} is lower), $T_{\text{"intermediate-temperature" storage tank}}$ decreases and, thus, pump *P2* is disabled; conversely, when $T_{\text{"intermediate-temperature" storage tank}}$ decreases, if there is availability of solar thermal energy, pump *P1* is activated, in order to employ the solar energy to raise $T_{\text{"intermediate-temperature" storage tank}}$. Please note that, in Figure 26, are displayed also the temperature of the DHW storage tank, to provide a better understanding of results presented in Section 3.2 as well as the operation modes and control procedures listed in Section 2.2.

Figure 18c, Figure 20c and Figure 22c provide insights in the coupling between the heat pump and the PVT panels. In particular, the water flow rate elaborated by pump *P1* is displayed, to support the above-mentioned discussion concerning the relationship between the temperature of the "*intermediate-temperature*" storage tank and the PVT panels. It is worth noting that, as stated in Section 2.2, in the operation *mode#3* pump *P1* has been activated from 19:00 untill 24:00, in order to lower the temperature of the "*intermediate-temperature*" storage tank and, thus, to increase the *PVT* performances. The *PVT* temperature is related to the ambient conditions and the operating parameters (i.e., the water flow rate and the water temperatures): when T_{amb} starts raising, the *PVT* temperature increases and, thus, *P1* is activated to transfer heat from the *PVT* panels toward the "*intermediate-temperature*" storage tank, thus lowering the *PVT* panel temperature and increasing T_7 and T_8. The operating conditions and the performance of the PVT panels are further described in Figure 19a, Figure 21a and Figure 23a, which focus on the relationship between the operating conditions and the

performances of the PVT panels (viz. the electrical and thermal power produced by the PVT panels). It is worth noting that the thermal power produced by the *PVT* panel is negative in Figure 23a, from 19:00 untill 24:00, owing to the above-mentioned control strategies (e.g., lower the temperature of the "*intermediate-temperature*" storage tank): these values find their corrispective daily-averaged values in Figure 17. In addition, Figure 19b, Figure 21b and Figure 23b compares the performance of the PV and PVT panels: (a) the electrical production of the PV and PVT panels is comparable; (b) PVT panels tend to have lower temperature in the second part of the day (approximately form 12:00 tilll the end of the day) and, thus, higher electrical power production (and, vice-versa for the first part of the day) these results are better visualized and commented in Section 3.3.3, to whom the reader should refer.

Finally, Figure 19c, Figure 21c and Figure 23c display the instantaneous values of the electrical power produced or consumed by the different component of the system. The aim of these figures is two-fold: (a) support the seasonal-time scale results reported in Figure 3.2.1 and (b) provide a better description on the influence of the auxiliaries on the system performances. The influence of the auxiliaries consumption on system performances provided in terms of daily-averaged quantities (in Section 2.4.1) is in agreement with the instantaneous values displayed here. In conclusion, it can be stated that the multifunctional heat pump systems was able to adjust its operating conditions accordingly to the changes in the boundary conditions related to the external ambient and to the different system components (i.e., storage temperatures, PVT operating condition, internal set-point temperatures, …). The flexible operation of the heat pump can be observed by the data displayed in Figure 10, which reflect in the performance presented in Figure 18a, Figure 20a and Figure 22a and in Figure 18b, Figure 20b and Figure 22b, owing to the variable speed compressor and the electronic expansion valve (see the details in Section 2.1). In addition, it was observed that the heat pump operation was correctly integrated, by using propter control systems, to the other system components (i.e., PVT panels, "*intermediate-temperature*" storage tank, …). The flexible operation of the heat pump, in the different instantaneous condition, resulted in the daily averaged performance presented in Section 3.2.

620

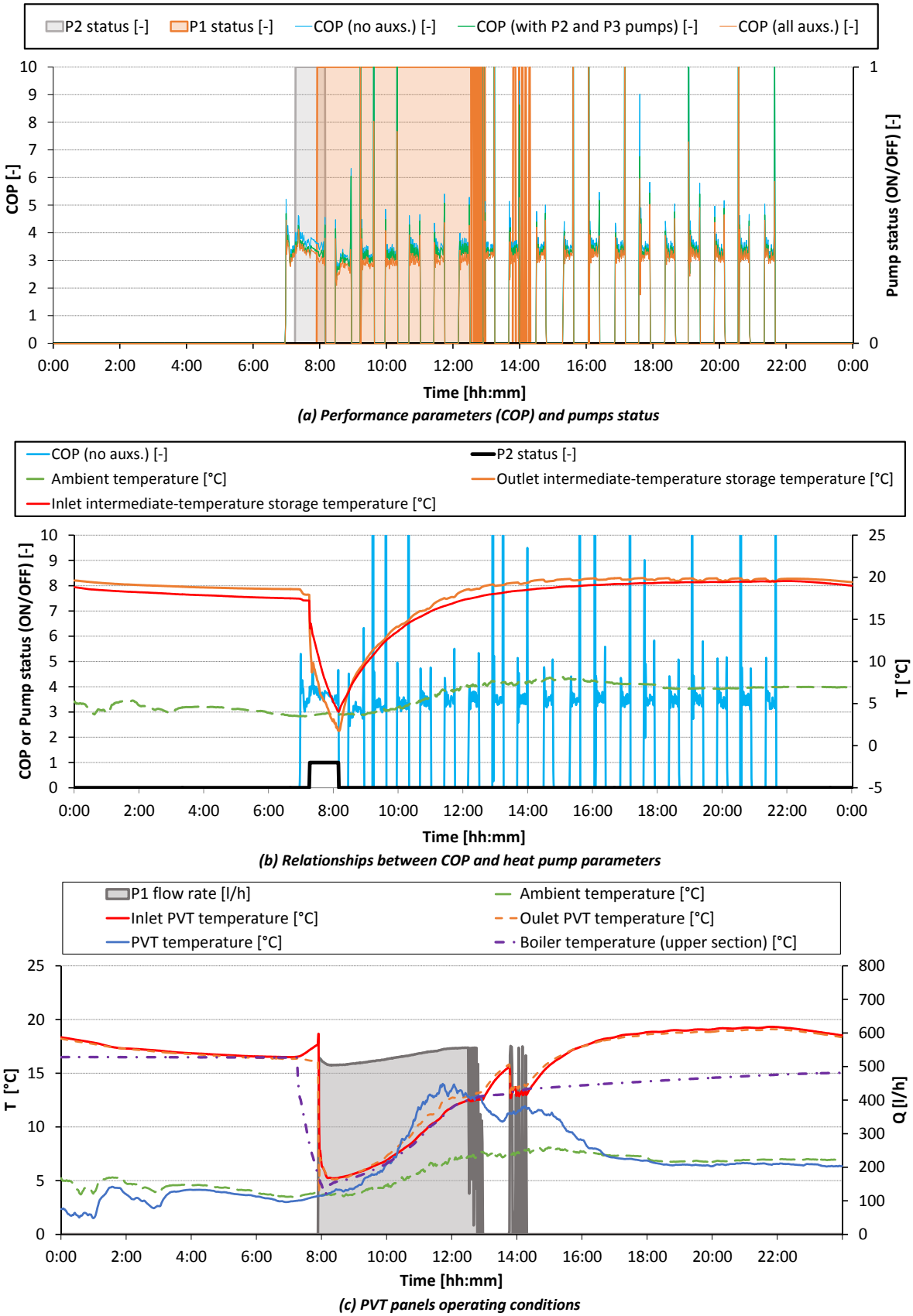

621 **Figure 18. Details on operation *mode#1* parameters – Part A (data obtained at 13/02/2017)**

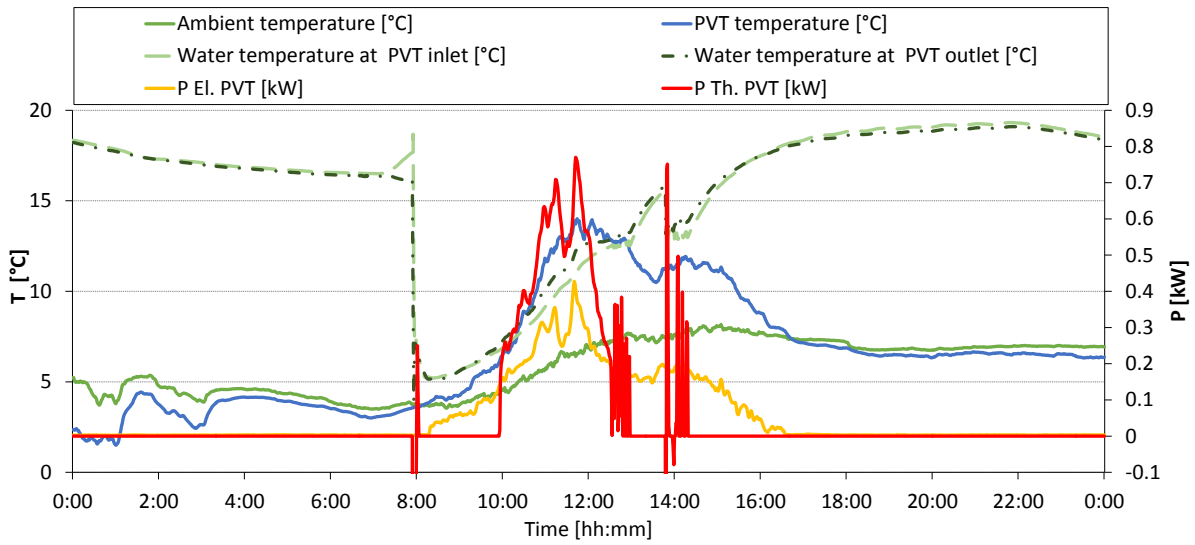

(a) Relationships between PVT operating conditions and performances

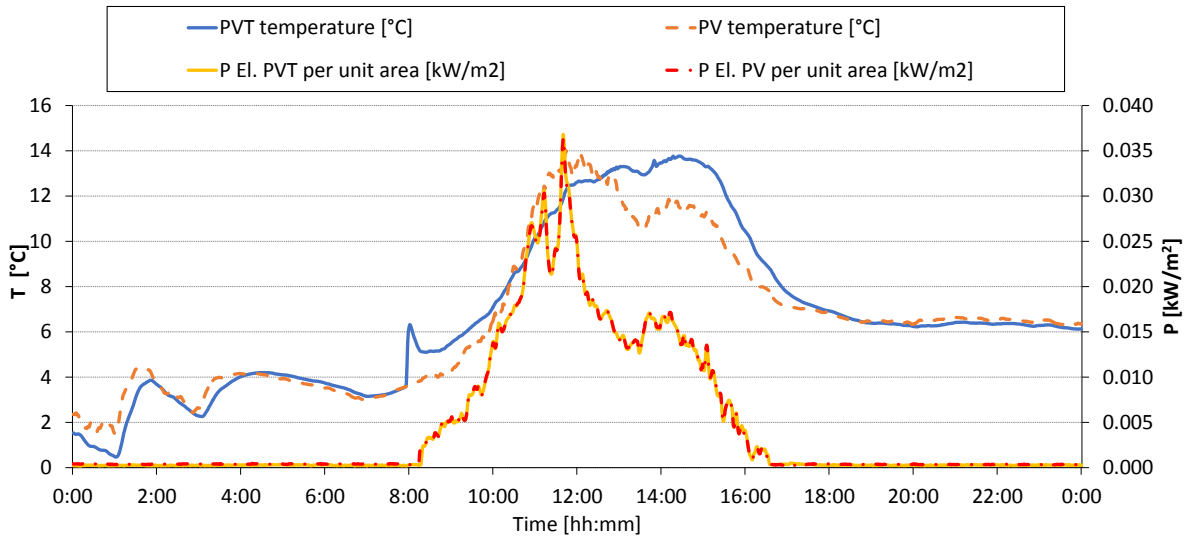

(b) Comparison between PV and PVT panels

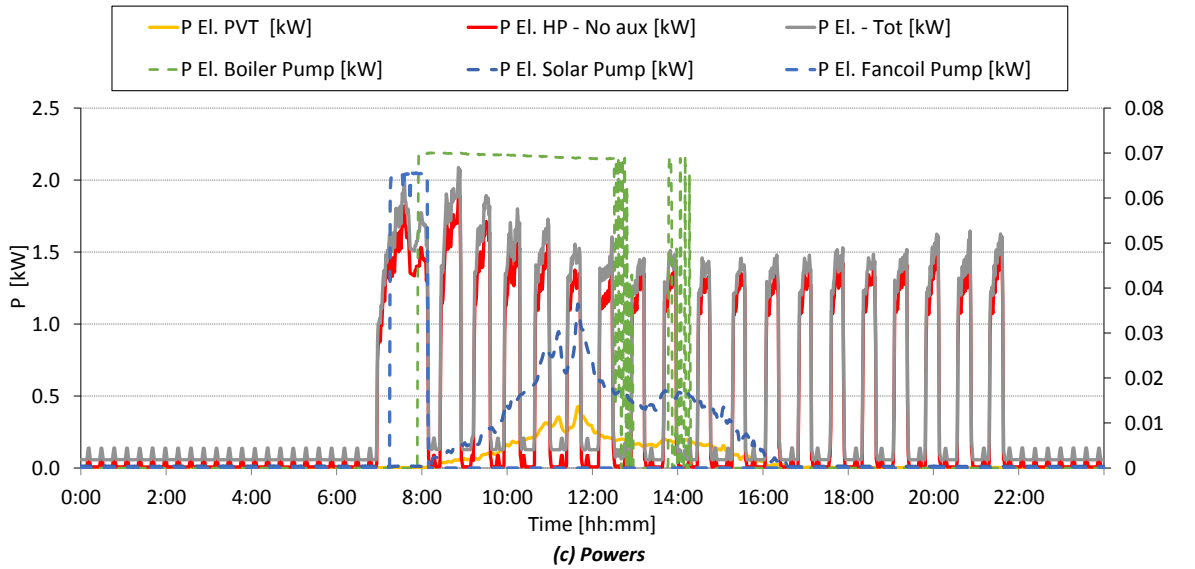

(c) Powers

Figure 19: Details on operation *mode#1* parameters – Part B (data obtained at 13/02/2017)

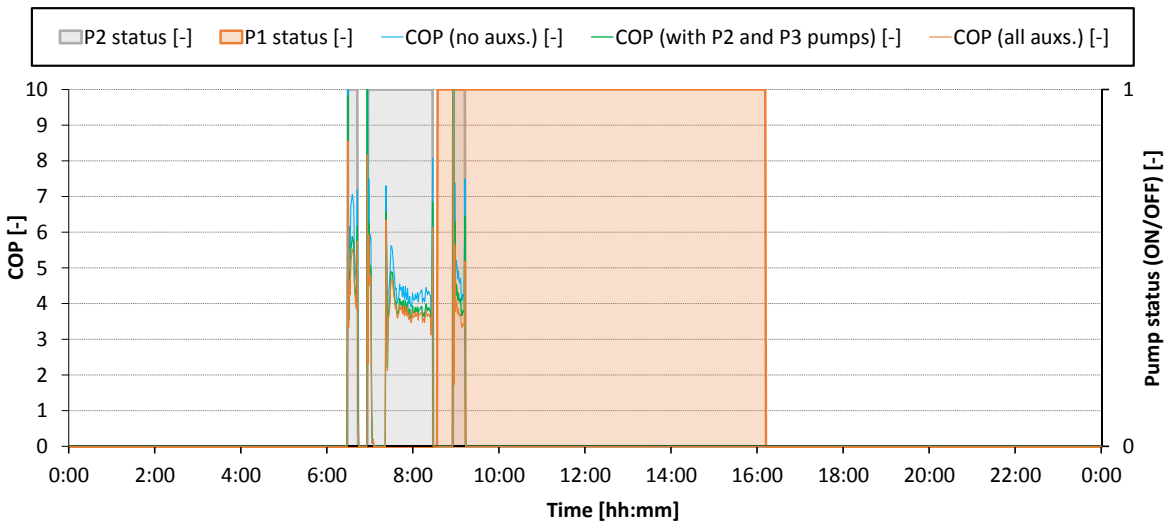

(a) Performance parameters (COP) and pumps status

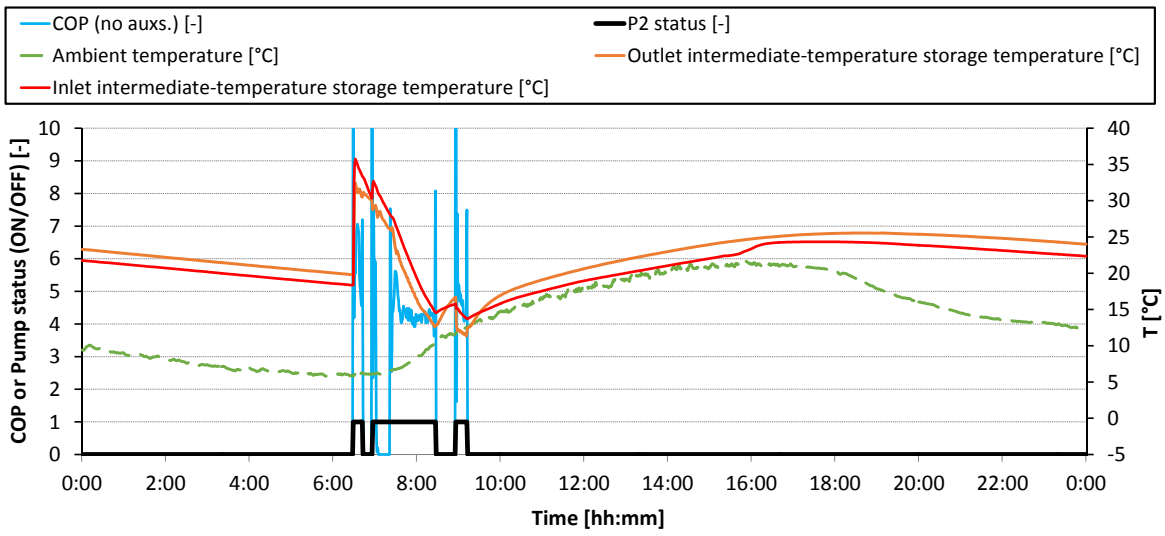

(b) Relationships between COP and heat pump parameters

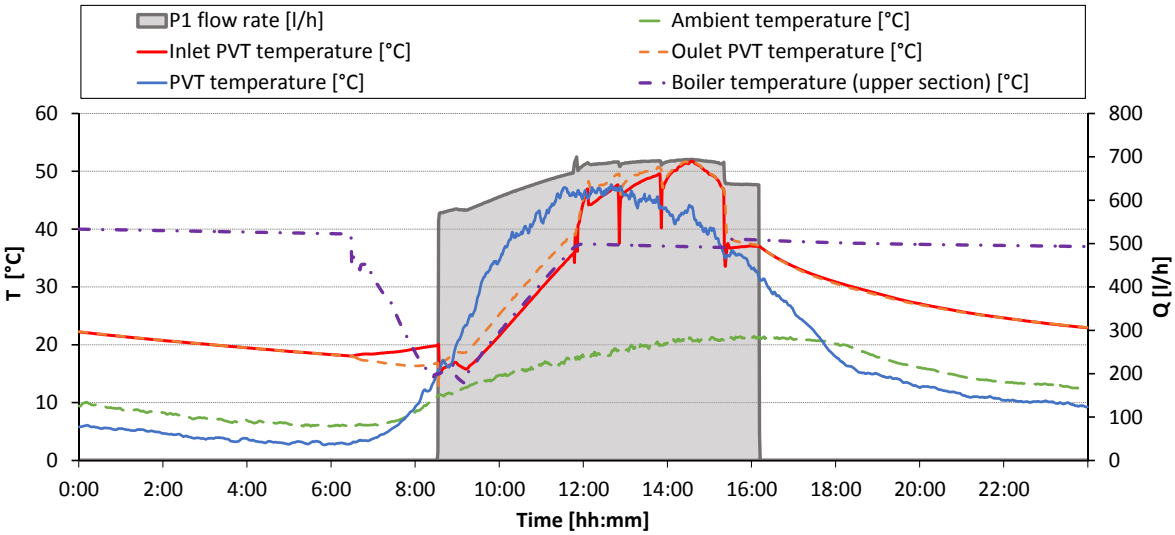

(c) PVT panels operating conditions

Figure 20: Details on operation *mode#2* parameters – Part A (data obtained at 17/03/2017)

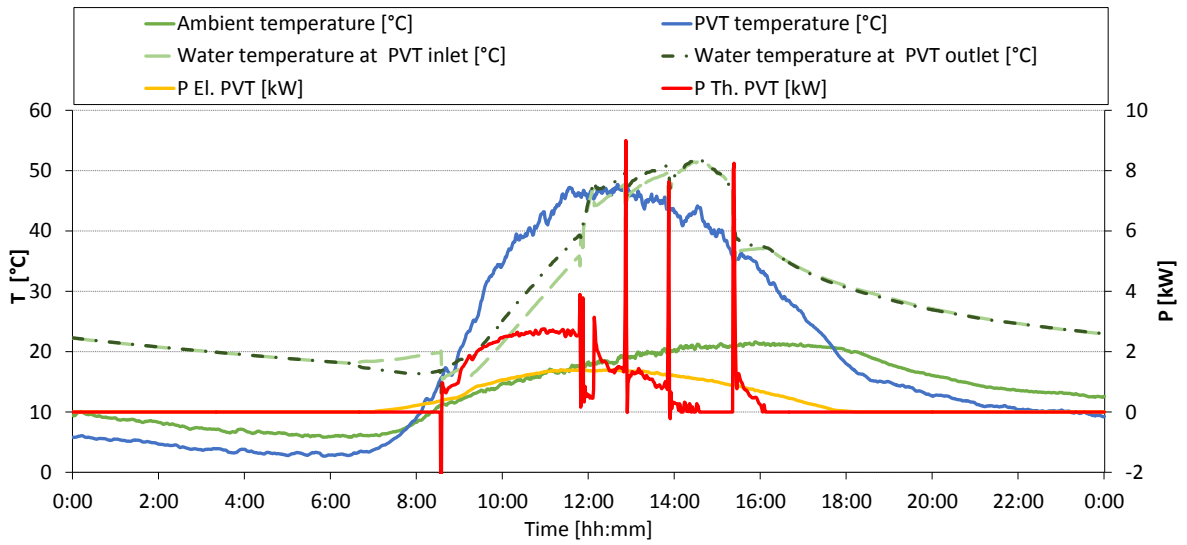

(a) Relationships between PVT operating conditions and performances

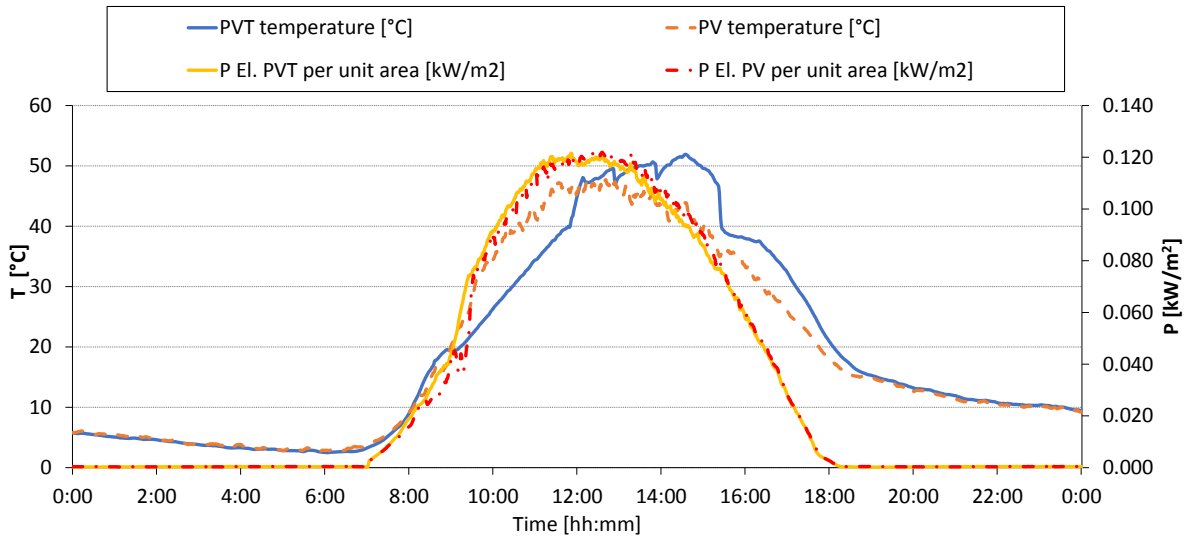

(b) Comparison between PV and PVT panels

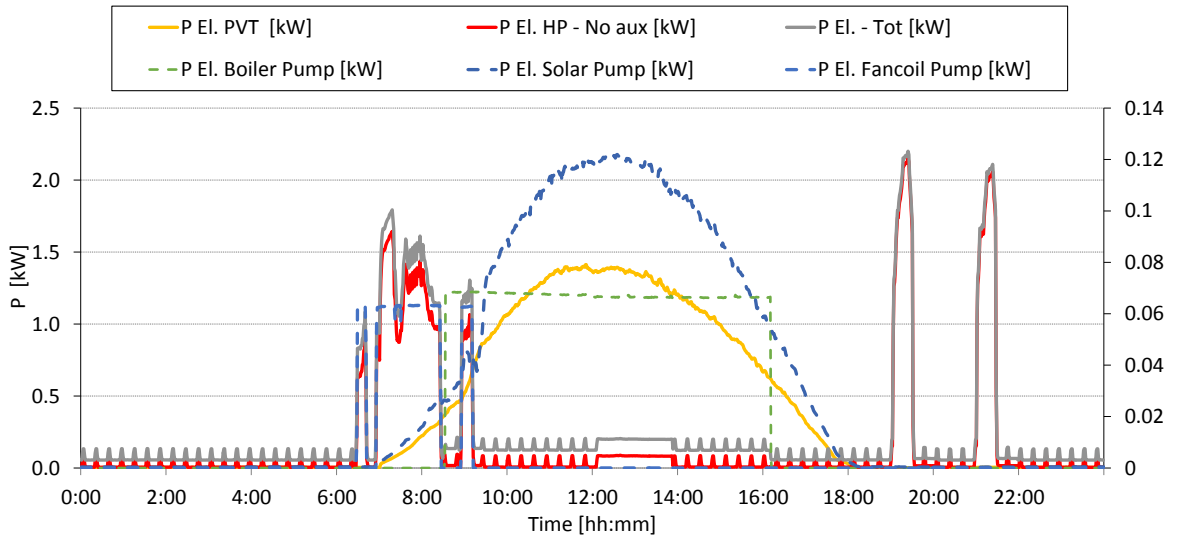

(c) Powers

626 **Figure 21- Details on operation *mode#2* parameters – Part B (data obtained at 17/03/2017)**

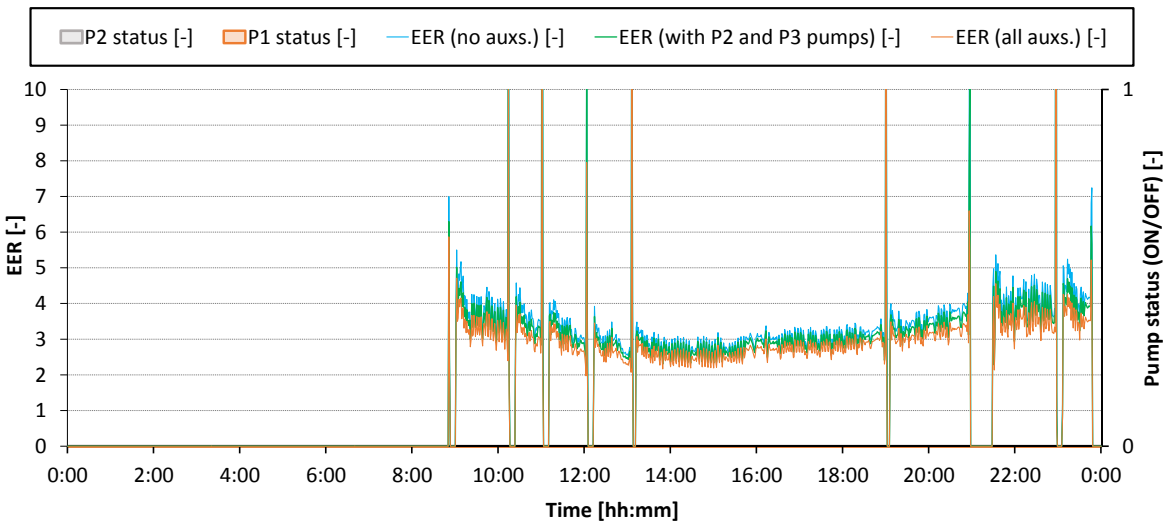

(a) Performance parameters (COP) and pumps status

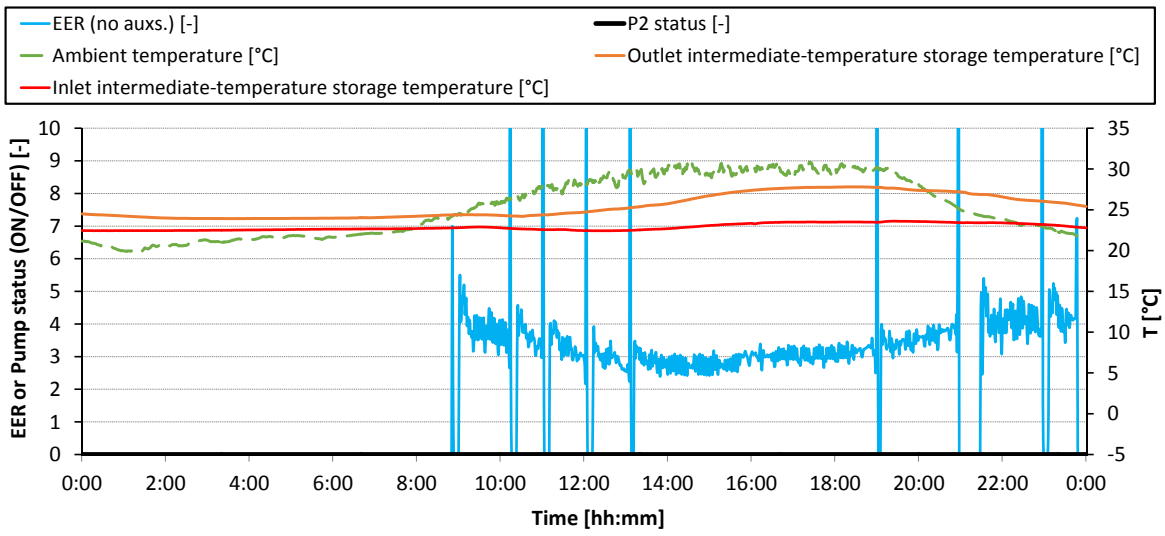

(b) Relationships between COP and heat pump parameters

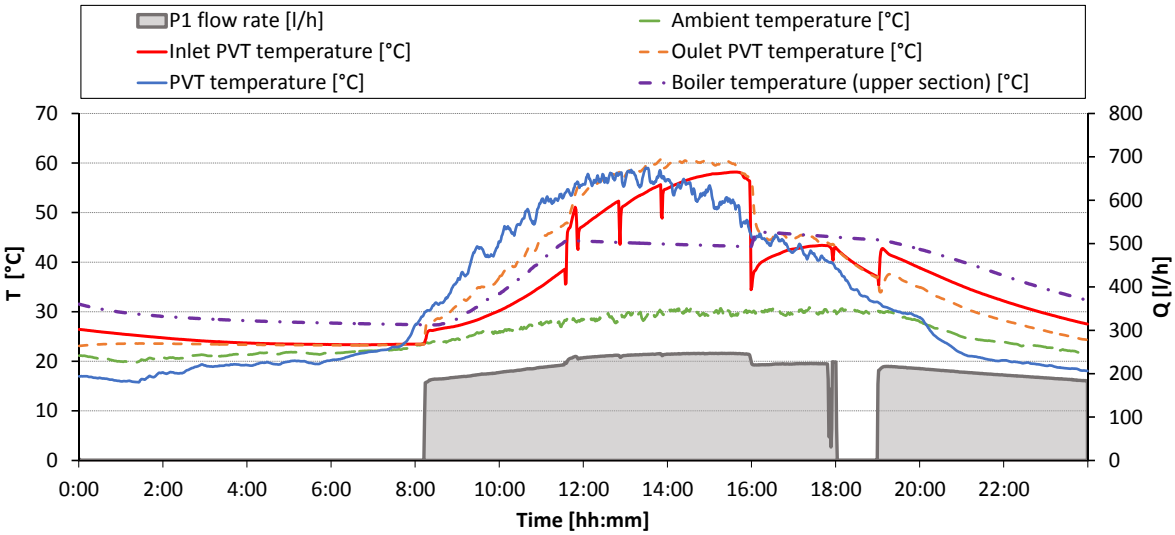

(c) PVT panels operating conditions

627 **Figure 22. Details on operation *mode#3* parameters – Part A (data obtained at 17/07/2017)**

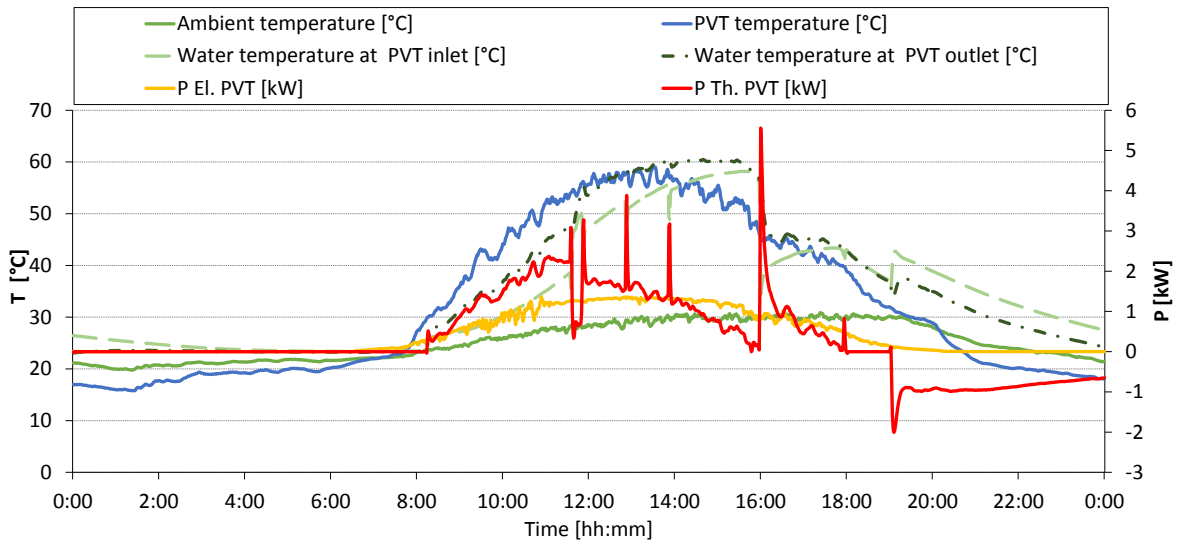

(a) Relationships between PVT operating conditions and performances

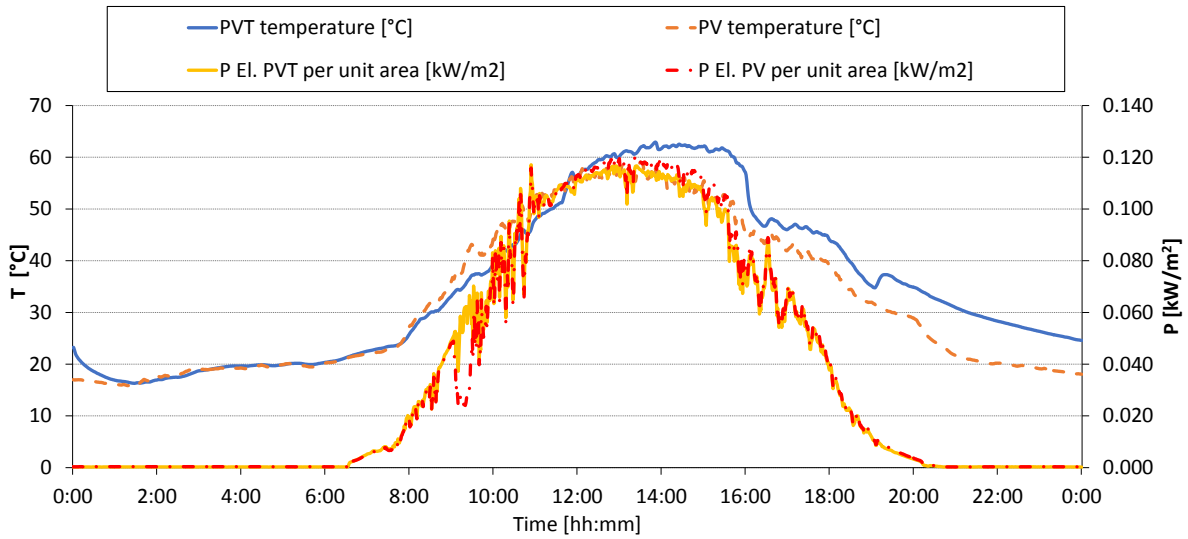

(b) Comparison between PV and PVT panels

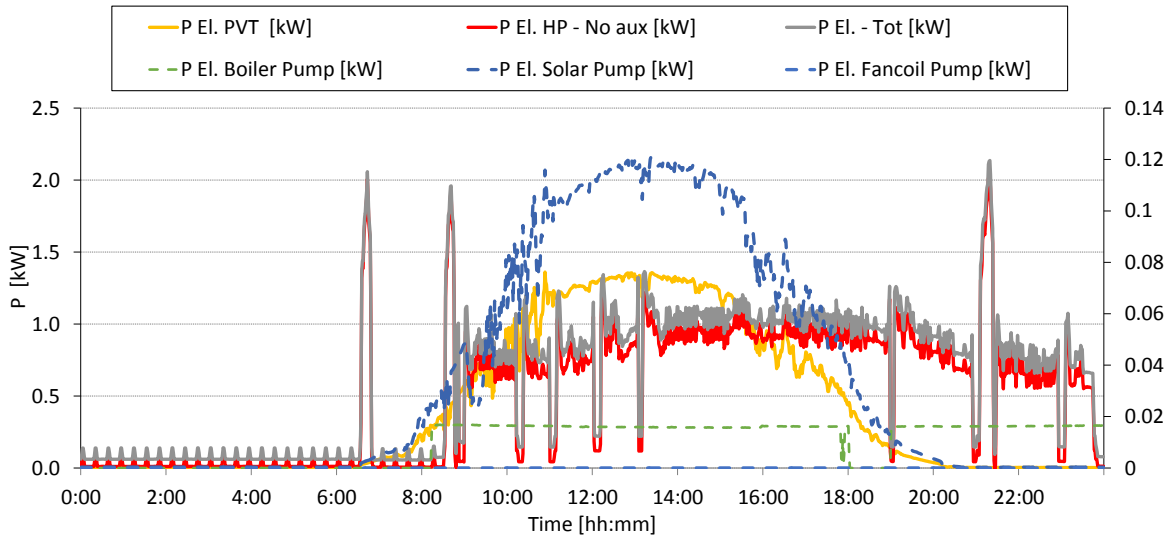

(c) Powers

628 **Figure 23. Details on operation *mode#3* parameters – Part B (data obtained at 17/07/2017)**

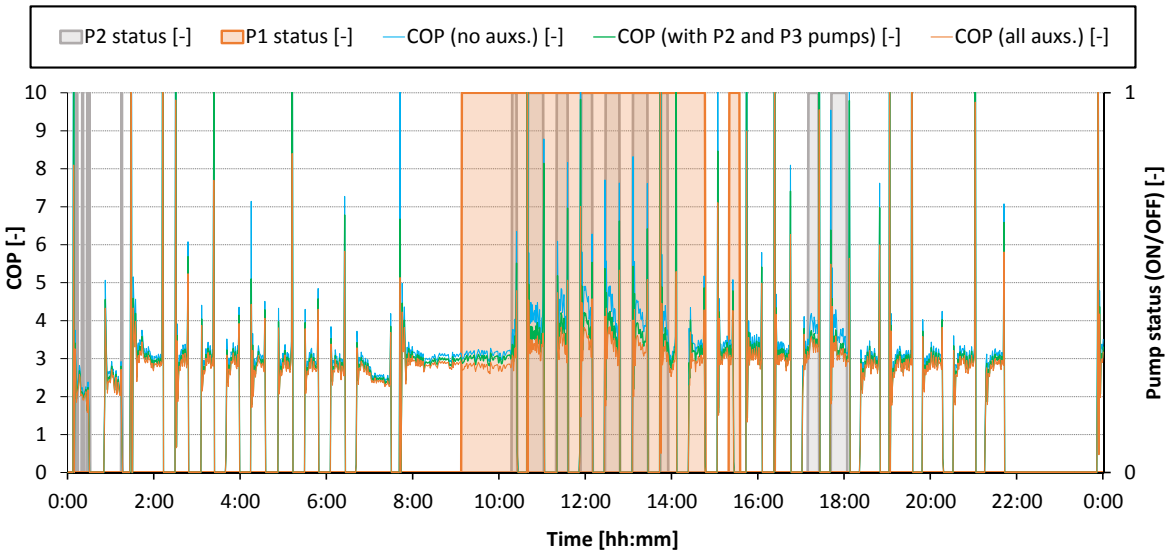

(a) Performance parameters (COP) and pumps status

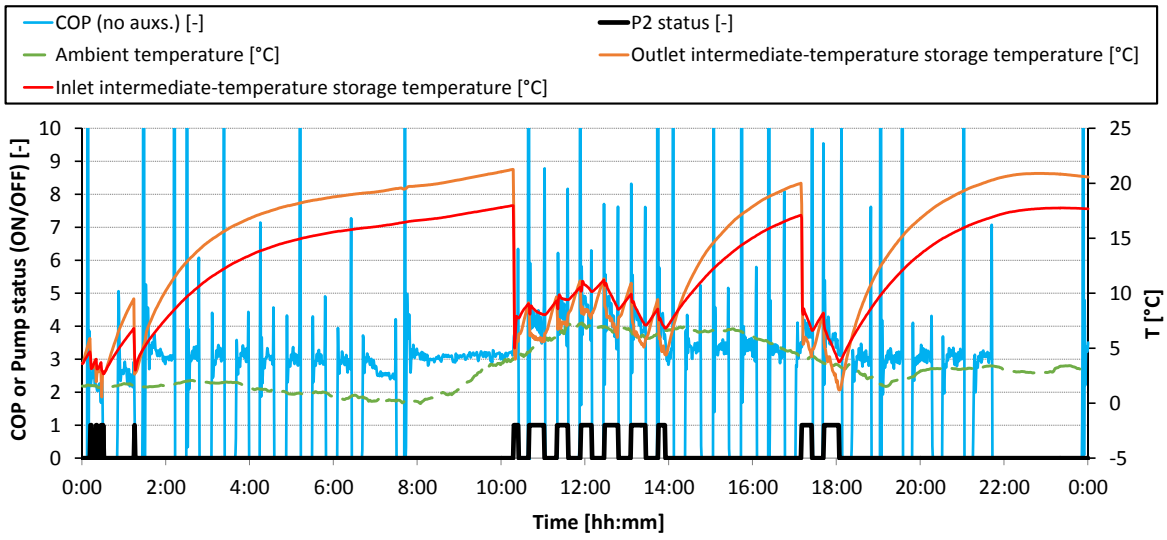

(b) Relationships between COP and heat pump parameters

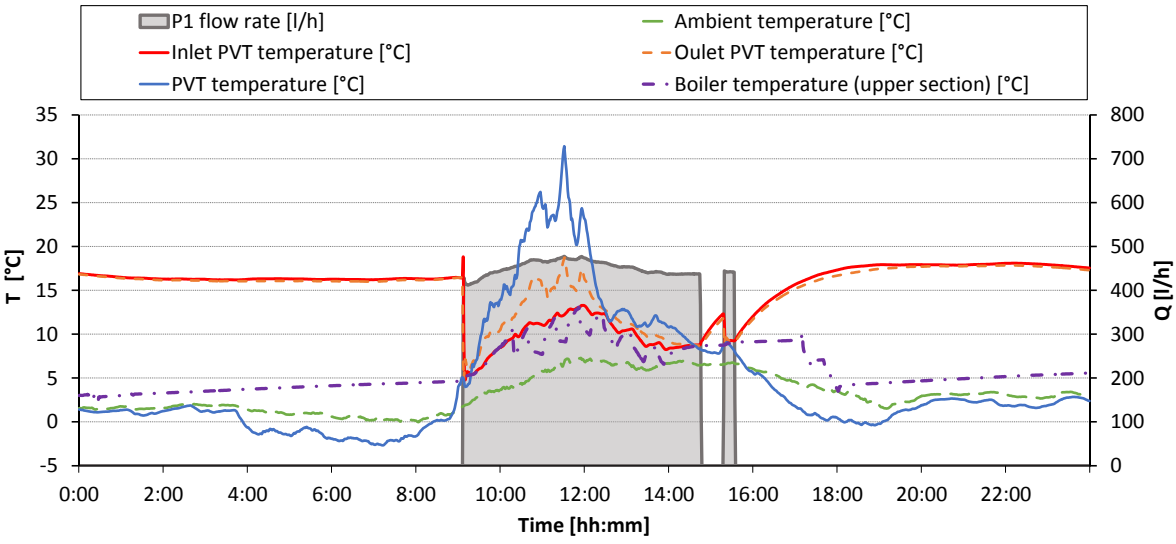

(c) PVT panels operating conditions

629 **Figure 24. Details on operation *mode#4* parameters – Part A (data obtained at 17/07/2017)**

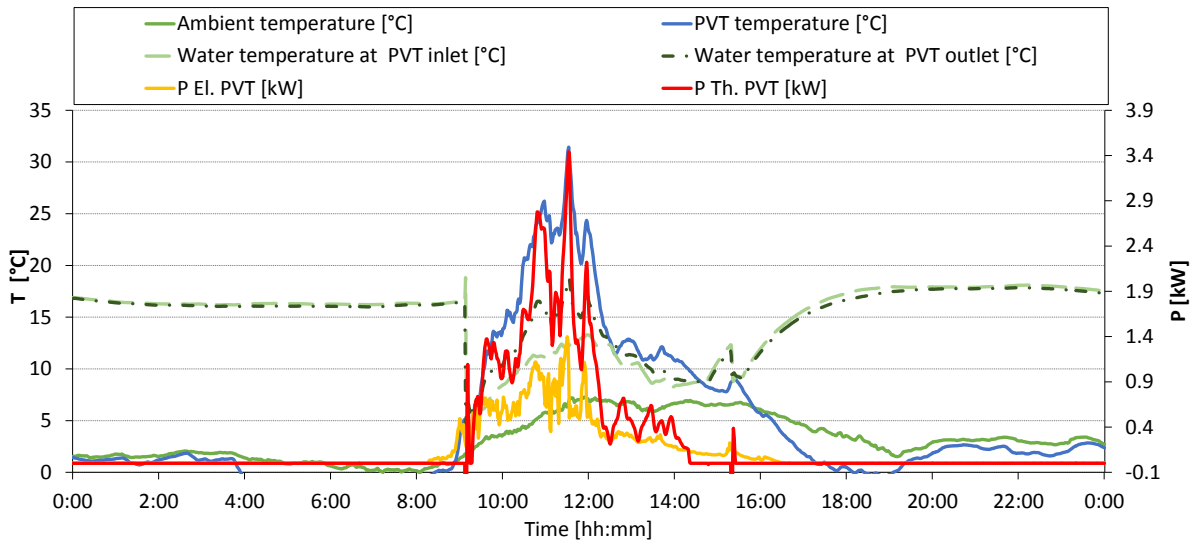

(a) Relationships between PVT operating conditions and performances

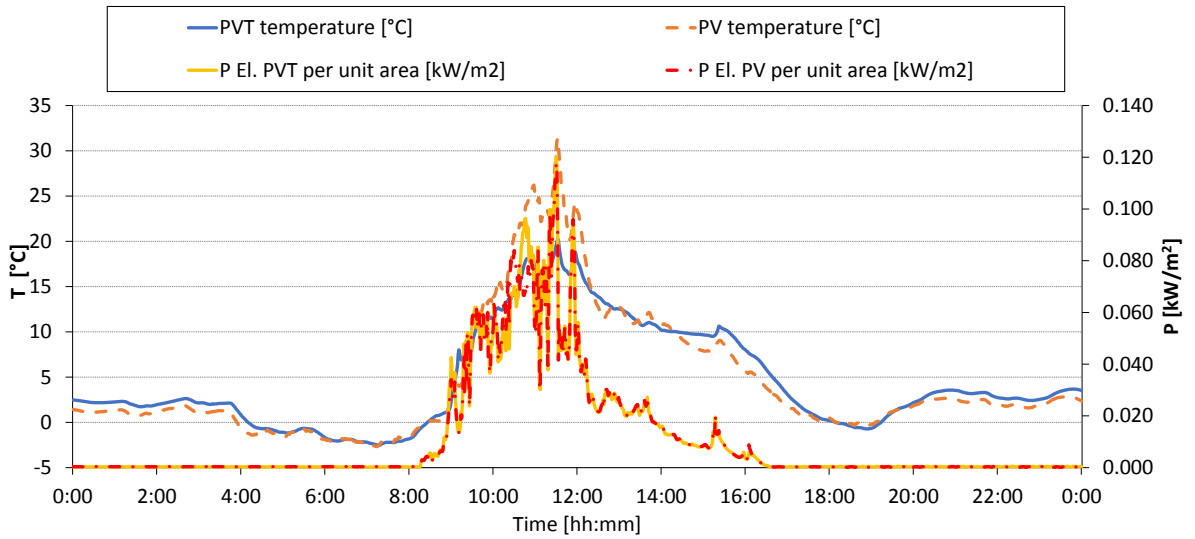

(b) Comparison between PV and FVT panels

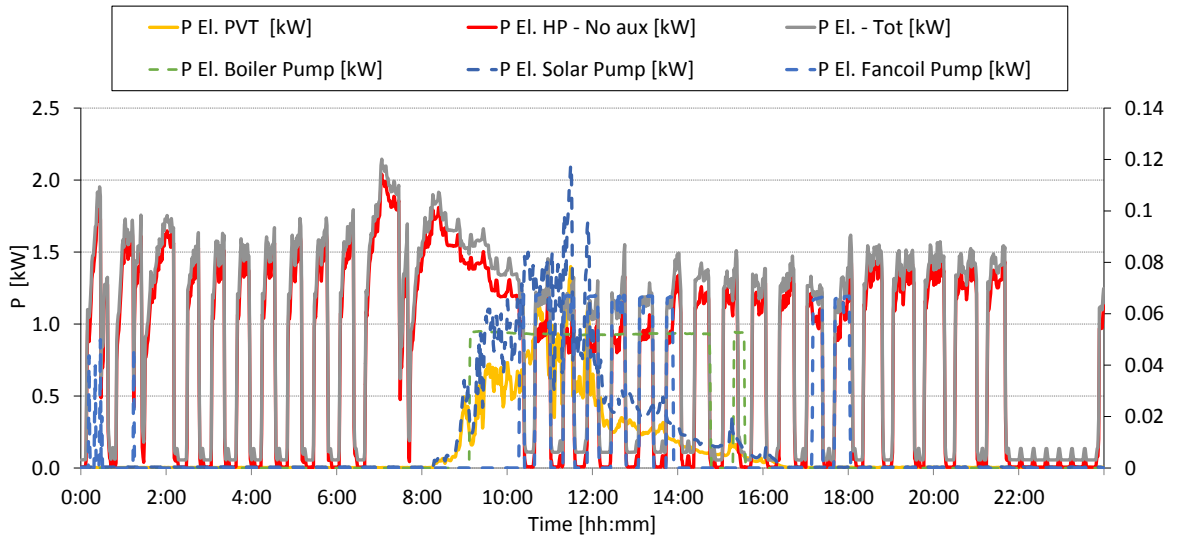

(c) Electric powers

630 **Figure 25. Details on operation *mode#4* parameters – Part B (data obtained at 17/07/2017)**

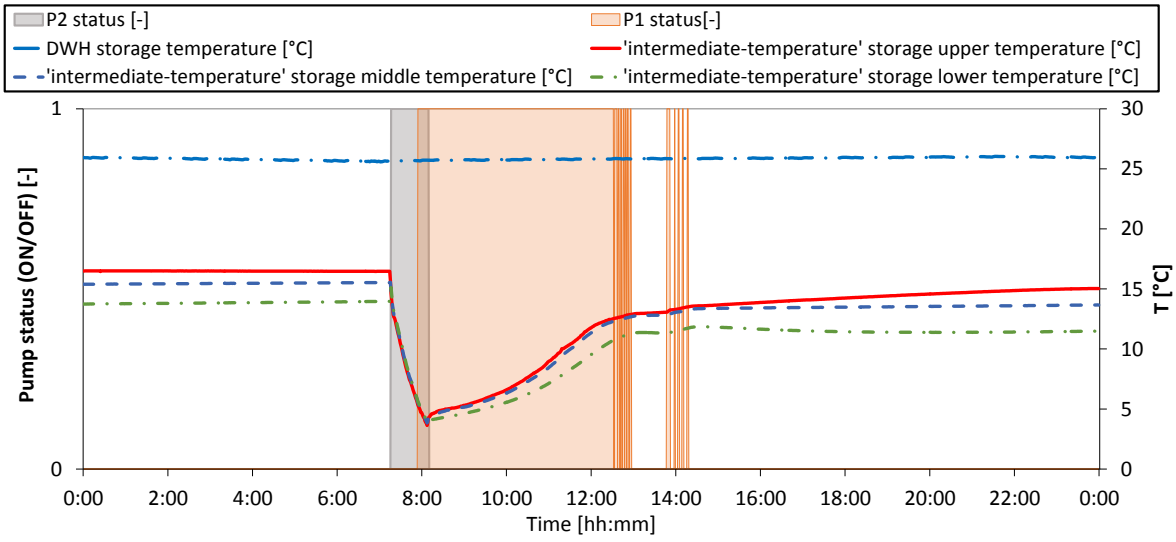

(a) operation mode#1 - data obtained at 13/02/2017

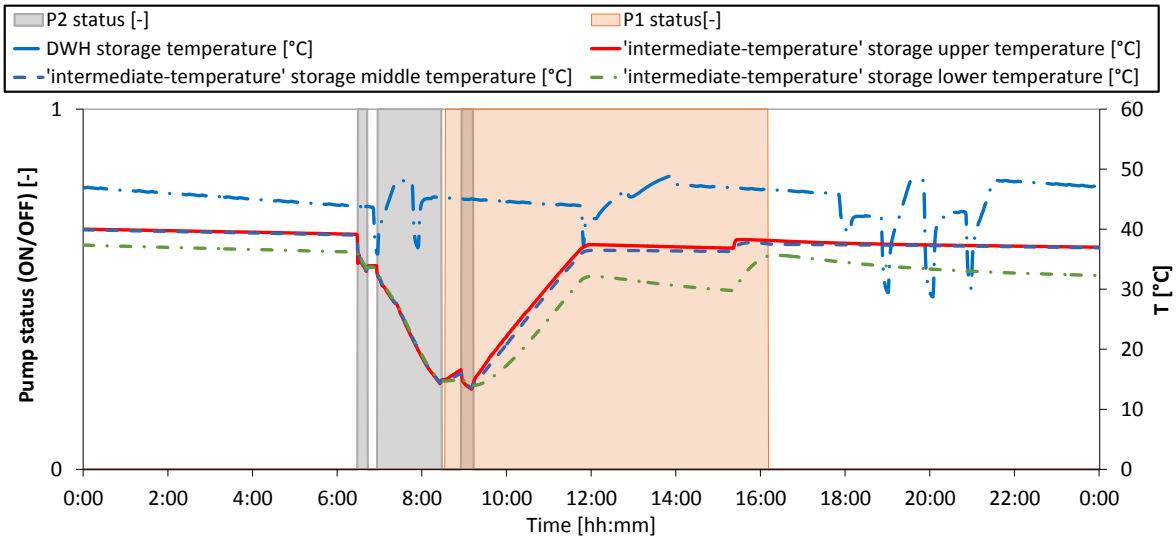

(b) operation mode#2 - data obtained at 17/03/2017

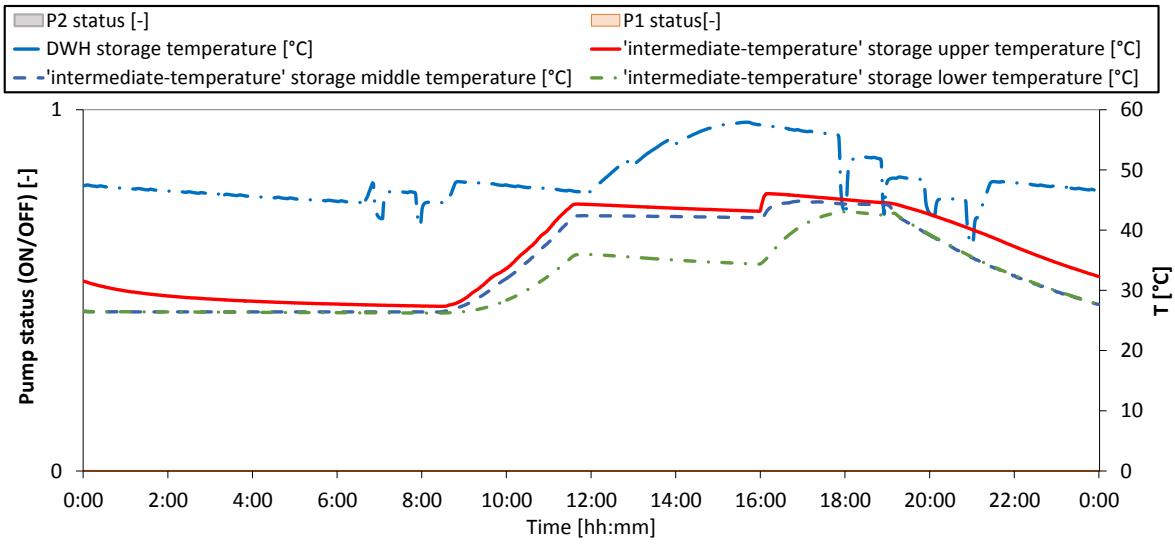

(c) operation mode#2 - data obtained at 17/07/2017

631 **Figure 26. DHW and "*intermediate-temperature*" storage tank temperatures**

3.3.2 Comparison between water source and air source

In this section, a more detailed discussion concerning the performance of the system is proposed, by analyzing the contribution of the "*water-source*" evaporator and the "*air-source*" evaporator to achieve the averaged performances described in Section 3.2.1 and Section 3.2.2. In particular, Figure 27 displays the significant increase of *COP*, owing to the use of the "*water-source*" evaporator; this figure extend some of the consideration previously presented in Figure 18a, Figure 20a and Figure 22a. It can be observed that, in Figure 27a, by activating the pump *P2* at 8.00 AM the *COP* increases from 2.7 to 8 (instantaneous values). Similar considerations can be drawn for the other days (Figure 27b and Figure 27c). The reasons behind the COP increase are quite known: *COP* increases owing to the lower difference between the evaporating and the condensing pressures (i.e., see Figure 10). It is important to remark that the "*water-source*" evaporator avoided the defrost cycles of the aerothermal heat pumps and, thus, the subsequent decrease in the performances. In this respect, the reader may refer to the defrost-related issues described by Zhang et al. [12]. It should be noted that the *COP* obtained using "*water-source*" has been obtained in the morning periods, which are the most unfavorable conditions owing to (a) high building load, (b) higher supply water temperature (T_3) and (c) lower T_{amb}. Unfortunately, the use of the "*water-source*" is limited in time and depends on the thermal energy available in the "*intermediate-temperature*" storage tank, as stated in Section 3.3.1 and displayed in Figure 18b, Figure 20b, Figure 22b and Figure 26. Future studies should be focused on alternative technical solutions for storage tanks (i.e., phase change material, *PCM*, storage tanks), to improve the availability of the "*water-source"*.

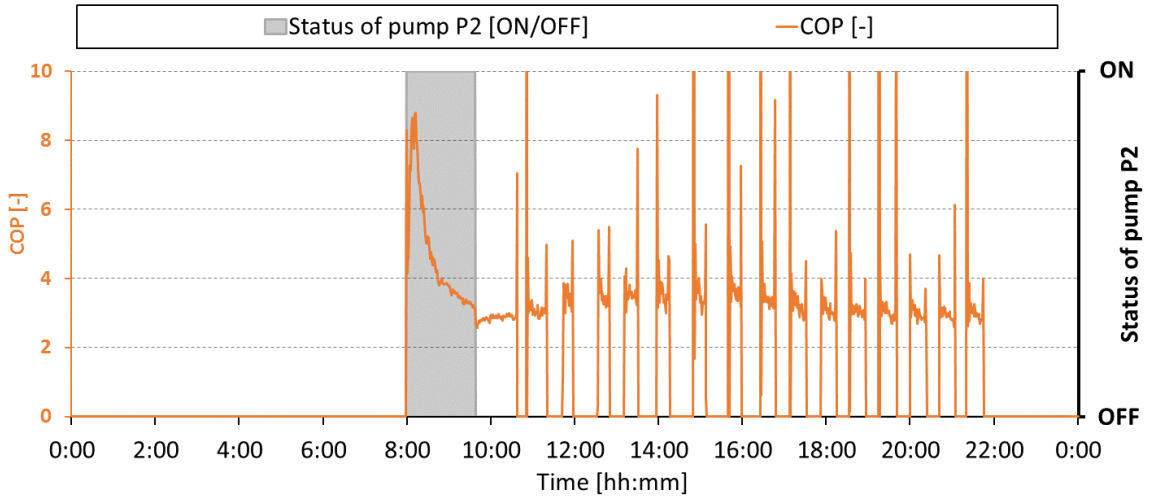

(a) data obtained at 17/01/2017, operation mode *mode#1*

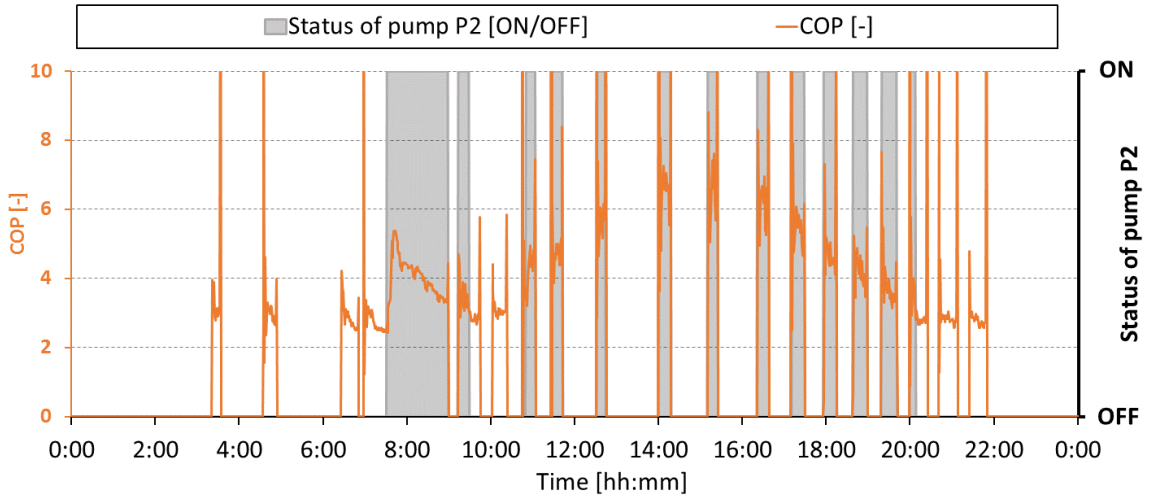

(b) data obtained at 23/01/2017, operation mode *mode#1*

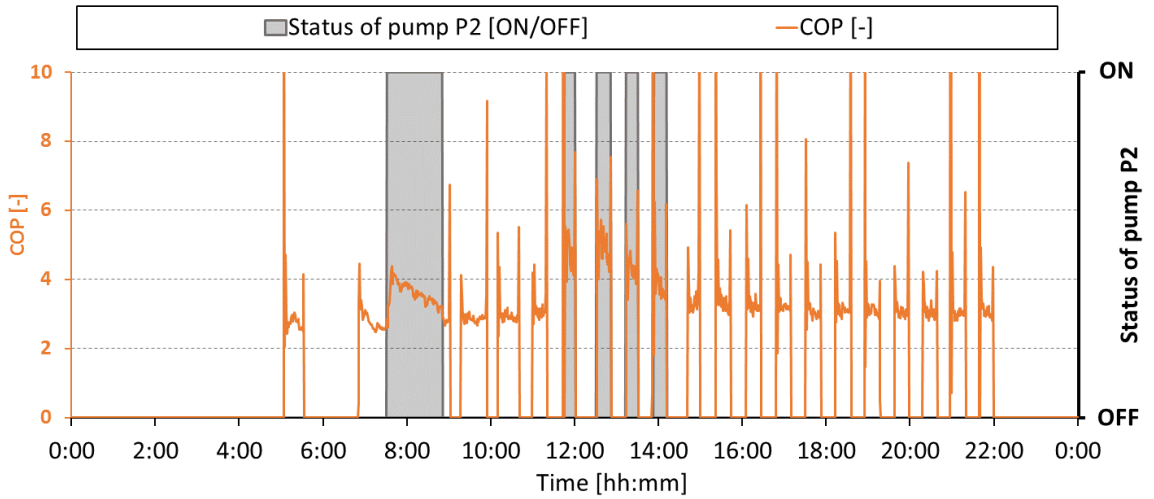

(c) data obtained at 27/01/2017, operation mode *mode#1*

651 **Figure 27: Daily performance of the multifunctional heat pump: influence of "*water-source*" and "*air-***

652 ***source*" evaporators**

3.3.3 Comparison between PV and PVT panels

In this section, a more detailed comparison between the performance of the *PV* and *PVT* panels is proposed, to better understand the averaged performance described in Section 3.2.3. In particular, Figure 28 compares the cell temperatures ($T_{cell,PVT}$ and $T_{cell,PV}$) and electrical power produced by the PVT (Eq. (8)) and PV (Eq. (10)) panels; this figure extend some of the consideration previously presented in Figure 19b, Figure 21b and Figure 23b; the drop of performance of PVT panels in the morning is caused by a shadow of a tree nearby the detached house. The discussion concerning the relationship between the ambient conditions and the cell temperatures were proposed before and it is not repeated here. It was observed that the *PVT* panels tend to have lower temperature in the first part of the day (approximately form 12:00 tilll the end of the day) and, thus, higher electrical power production (and, vice-versa for the first part of the day) these results are better visualized and commented in Section 3.3.3, to whom the reader should refer. The electrical power production of the panels are related to the cell temperatures, owing to the well-known relationships between temperature and *PV* efficiency (see, for example ref. [40]). In conclusion, Figure 28 contributes and support the previous discussion proposed in Section 2.3 considering the relationship between the electrical power production and the cell temperatures. It can be stated that the electrical production of the PVT panels is comparable to the one of the PV panels. In addition, the PVT panels support the whole system by providing thermal energy to the "*intermediate-temperature*" storage tank. Future studies may be devoted to use the present experimental data to validate numerical model to predict the performance of *PVT* panels.

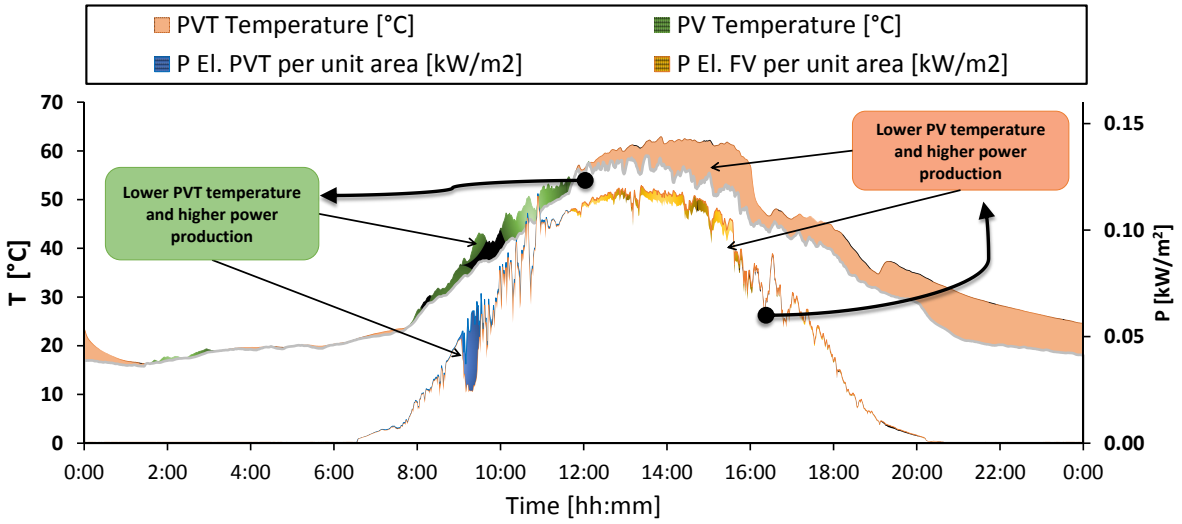

(a) data obtained at 10/07/2017

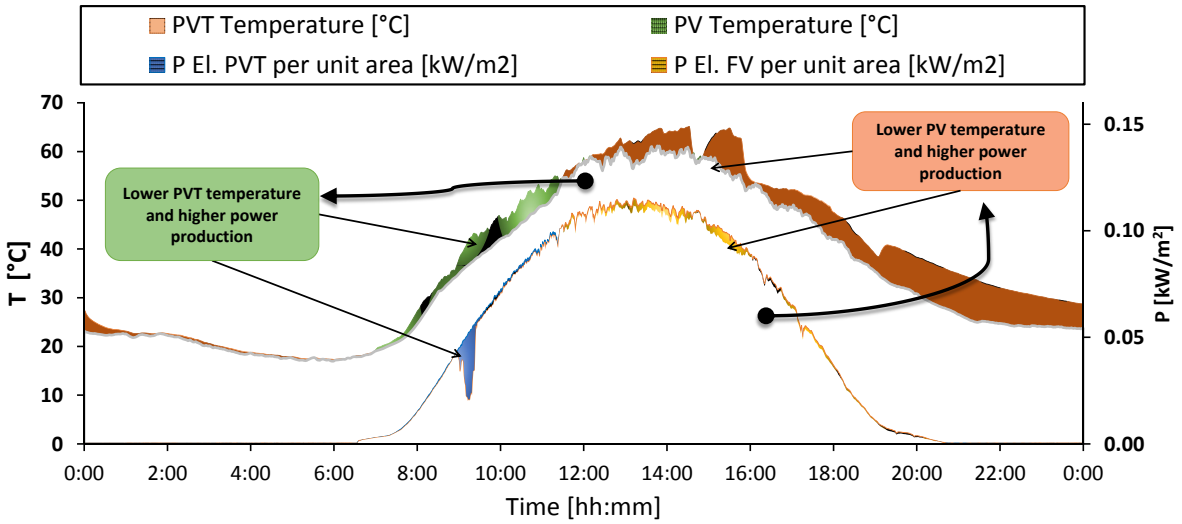

(b) data obtained at 13/07/2017

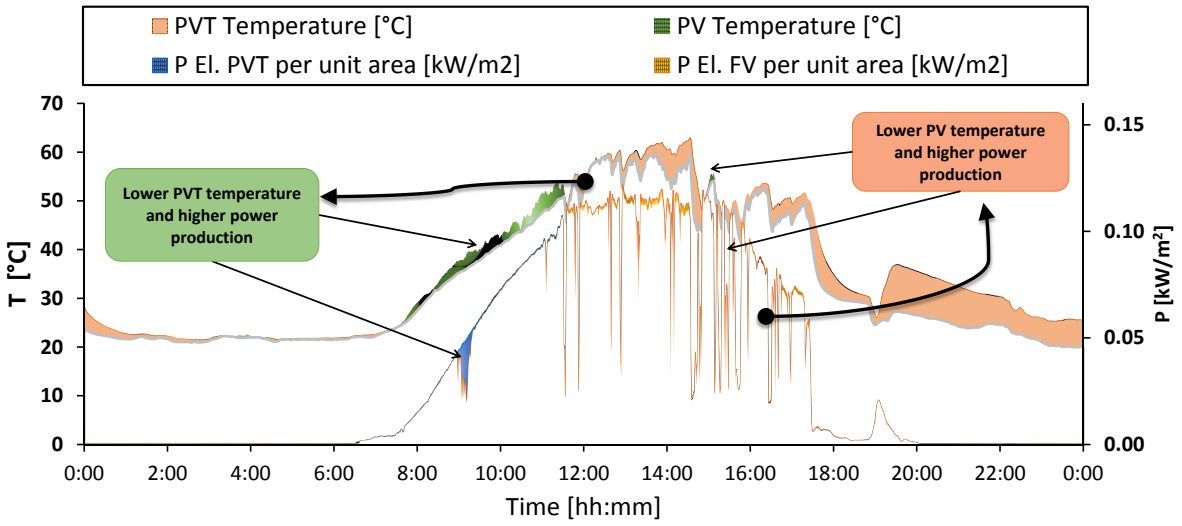

(c) data obtained at 17/07/2017

671 **Figure 28: Comparison between PV and PVT panels**

4 Comparison with an air-to-water single-source multifunctional heat pump

In the previous paragraphs, the performance of the present dual source multifunctional heat pump was detailed (Section 3.2.1 and Section 3.3.1); subsequently, the performance improvements, owing to the "*water-source*" evaporator and to the PVT panels was described (Sections 3.2.2-3.2.3 and Sections 3.3.2-3.3.3). The aim of this section is to propose a simple and straightforward comparison between the present dual source multifunctional heat pump and an air-to-water single-source multifunctional heat pump (called "*baseline*" in the following), working under the same boundary conditions (viz. the monitored period). The baseline system is composed by PV panels and a reversible air-to-water heat pump, which should be used to produce *DHW* and for heating/cooling purposes. The main assumption employed in this comparison are the followings: (a) the "*baseline*" system is equipped with PV panels that ensures an electrical production equal to the one of the PVT panels (which is reasonable owing to the results discussed in Section 3.2.3); (b) the performances of dual source multifunctional heat pump is the same as the "baseline" system, when working in the heating mode with the "*air-source*" evaporator, when working in the cooling mode and when producing DHW with the heat pump; (c) the operating conditions of the two systems are the same as the ones in the monitored period. The first assumption allows to neglect the electrical production of the *PVT* and *PV* panels; the second assumption allows the performance comparison as described below; the third assumptions allows a straightforward comparison, as boundary conditions are set (i.e., the values in Table 8).

Based on the three above-mentioned assumptions, the comparison is performed as follows: (a) the energy consumption of the heat pump in the "*water-source*" conditions is replaced with the equivalent energy consumption with "*air-source*" conditions (viz. Equivalent "*water-source*" conditions); (b) $Q_{PVT \rightarrow DHW-tank}$ (the heat provided by the PVT panels to the *DHW* tank) should be replaced by the equivalent energy consumption of the heat pump (viz. equivalent "*PVT-DHW*" conditions). In particular, the calculation procedure is described below:

1. **Equivalent "*water-source*" conditions.** When the present multifunctional heat pump employs the "*water-source*" evaporator, it has an electric energy consumption equal to $E_{el,PdC,water-source}$ with a mean performance equal to $\overline{COP_{"water-source"}}$ (as displayed in Table 8); in this condition, the heat pump provides a thermal energy ($En_{th,PdC}$) equal to:

$$En_{th,PdC} = E_{el,PdC,water-source}\ \overline{COP_{"water-source"}} \quad (11)$$

If the heat pump would be operated with the "*air-source*" evaporator (instead of the "*water-source*"

evaporator), the corresponding electrical energy consumption ($E_{el,PdC,air-source}$) would be equal to:

$$E_{el,PdC,air-source} \approx \frac{En_{th,PdC}}{\overline{COP}_{\text{air-source},morning}} + n_{day} E_{el,defrost} \quad (12)$$

Where $E_{el,defrost}$ is the daily energy consumption owing to defrosts (when "*water-source*" evaporator is applied the defrosts are avoided). From Eq. (11) and Eq. (12) follows Eq. (13):

$$E_{el,PdC,air-source} \approx E_{el,PdC,water-source} \frac{COP_{"water-source"}}{\overline{COP}_{\text{air-source},morning}} + n_{day} E_{el,defrost} \quad (13)$$

Where $E_{el,defrost} \approx 0.1 \frac{kWh}{day}$ (obtained from the experimental measurements) and $\overline{COP_{water}}$ is taken from Table 8 for the operation *mode#1* and as a weighted-average value of *mode#1*, for the operation mode#2 .

2. **Equivalent "*PVT-DHW*" conditions.** The equivalent energy consumption ($E_{el,Baseline \to DHW}$) of the heat pump, needed to produce $Q_{PVT \to DHW\text{-}tank}$ is computed as follows (based on mean performance of the system, $\overline{COP}_{\text{air-source},DHW}$):

$$E_{el,Baseline \to DHW} \approx \frac{Q_{PVT \to DHW-tank}}{\overline{COP}_{\text{air-source},DHW}} \quad (14)$$

It si worth noting that, when using the baseline air-to-water single source heat pump, the consumption of pumps P1 and P2 should be neglected.; please note also that, in the operation *mode#2* no defrosts have been considered (conversely, they have been considered for the operation *mode#1* and *#4*). At this point, $COP_{"air-source"}$ and $COP_{"air-source"}$ need to be estimated and the model proposed by Madonna and Bazzocchi [11] is employed. This model considers the *COP* as a product of three terms: (a) full load efficiency (COP_{fl}); (b) part load factor (*PLF*); (c) degradation coefficient due to defrost operations (*DOF*); hence, the COP is computed as follows:

$$COP = COP_{fl} PLF\ DOF \quad (15)$$

The reader may refer to the work of Madonna and Bazzocchi [11] the definition of the above-mentioned coefficients; it follows that, in Eq. (13), $COP_{\text{air-source},morning} \approx 2$ and, in Eq. (14) $\overline{COP}_{\text{air-source},DHW} \approx 2.8$.

Therefore, based on Eqs. (11-15) and the monitored energy consumptions, the averaged *COP* of the "*baseline*" system as well as the daily-averaged energy consumptions can be computed, and the two systems can be compared. In particular, the results of this comparison are displayed in Table 9 (monthly-averaged performances) and Table 10 (operation mode-averaged performances): the proposed system, compared to the "*baseline*" air-to-water heat pump has, on averaged, 17.7% higher performance in the operation *mode#1*,

31.8% higher performance in the operation mode#2, 6.4% higher performance in the operation *mode#3* and 9.8% higher performance in the operation *mode#4*. In addition, the proposed system, compared with the "*baseline*" air-to-water heat pump has, on averaged, 15.4% lower daily-averaged energy consumptions.

Table 9. Comparison between the present dual source multifunctional heat pump and a "*baseline*" air-to-water single-source multifunctional heat pump (monthly-averaged performances)

Month	Operation mode	$\Delta COP_{Baseline\text{-}Sincler+}$ [-]	$\Delta EER_{Baseline\text{-}Sincler+}$ [-]	$\Delta E_{Day,\ Baseline\text{-}Sincler+}$ [kWh/day]
January	mode#1	14.8%	-	-12.5%
February	mode#1	15.6%	-	-12.8%
March	mode#1	36.4%	-	-25.2%
March	mode#2	64.0%	-	-36.4%
April	mode#2	68.6%	-	-38.2%
May	mode#2	55.1%	-	-32.8%
May	mode#3	-	25.9%	-20.0%
June	mode#3	-	19.2%	-15.8%
July	mode#3	-	5.6%	-4.8%
August	mode#3	-	12.7%	-11.0%
September	mode#3	-	11.3%	-9.7%
October	mode#4	52.8%	-	-31.2%
November	mode#4	16.8%	-	-13.7%
December	mode#4	12.6%	-	-11.0%

Table 10. Comparison between the present dual source multifunctional heat pump and a "*baseline*" air-to-water single-source multifunctional heat pump (operation mode-averaged performances)

Operation mode	$\Delta COP_{Baseline\text{-}Sincler+}$ [-]	$\Delta EER_{Baseline\text{-}Sincler+}$ [-]	$\Delta E_{Day,\ Baseline\text{-}Sincler+}$ [kWh/day]
mode#1	17.7%		-14.4%
mode#2	63.7%		-36.3%
mode#3		12.1%	-10.3%
mode#4	15.7%		-13.1%
Total	-	-	**-15.4%**

5 Conclusions, outcomes and outlooks

This paper presents the very first results of field study concerning a novel solar-assisted dual-source multifunctional heat pump, installed in a detached house in Milan, in three operation modes. The main results of the filed study are as follows:

- the averaged performance (*COP* and *EER*) of the multifunctional heat pump is approximately 3, in the three different operation modes;
- the use of "*water-source*" evaporator allows to significantly increase the performance of the plant (COP increases of approximately 34 %, compared with the "*air-source*") and to avoid defrost cycles;

- the thermal energy produced by the *PVT* panels were successfully used to support the production of *DHW* in the summer season; in particular, approximately 63% of the heat needed by the *DHW* storage tank has been ensured by the PVT panels;
- the *PVT* panels can successfully support the "water-source" evaporator in the winter/spring seasons;
- the proposed system, compared with the "*baseline*" air-to-water heat pump has on averaged, 15.4% lower daily-averaged energy consumptions.
- the electrical production of the PVT panels is comparable to the one of the PV panels. In addition, the PVT panels support the whole system by providing thermal energy to the "*intermediate-temperature*" storage tank.

Ongoing research as well as future studies may concern both experimental and numerical researches. On the experimental part, outlooks are as follows:

- relate the daily and the seasonal operations, to provide a multi-scale evaluation of the heat pump performance and propose a comprehensive thermodynamic evaluation (energy and exergy anlayisis) of the whole system;
- compare the performance of *PV* and *PVT* systems and provide insights in the relationships between operating conditions (i.e., temperatures, flow rates, ambient conditions) and the panels performances (i.e., thermal and electrical energy production);
- study alternative technical solutions for storage tanks (i.e., phase change material, *PCM*, storage tanks), to improve the availability of the "*water-source*".

On the numerical part, future studies would concern testing and validation of a TRNSYS approach, to extend the results of the present experimental study to different climatic conditions and, finally, to assess the economic feasibility of the proposed system.

Acknowledgements

This work has been financed by the Research Fund for the Italian Electrical System under the Contract Agreement between RSE S.p.A. and the Ministry of Economic Development - General Directorate for Nuclear Energy, Renewable Energy and Energy Efficiency stipulated on July 29, 2009 in compliance with the Decree of

764 March 19, 2009. The authors are also grateful to CLIVET Spa for elaborating and providing the heat pump
765 employed in the research activities.

766 **References**

767

[1] *Energy Roadmap 2050, COM(2011) 885 Final; European Commission,* 2011.

[2] *Directive 2002/91/EC on Energy Performance of Building Directive; European Commission,* 2002.

[3] *Directive 2010/31/EU Energy Performance of Building Directive; European Commission,* 2010.

[4] D. DÁgostino, B. Cuniberti et P. Bertoldi, «Data on European non-residential buildings,» *Data in Brief,* vol. 14, pp. 759-762, 2017.

[5] D. DÁgostino, B. Cuniberti et P. Bertoldi, «Energy consumption and efficiency technology measures in European non-residential buildings,» *Energy and Buildings,* vol. 153, pp. 72-86, 2017.

[6] *An EU Strategy on Heating and Cooling, COM(2016) 51 Final; European Commission: Brussels, Belgium, 2016,* 2016.

[7] D. Connolly, B. V. Mathiesen, P. A. Østergaard, B. Möller, S. Nielsen, H. Lund, D. Trier, U. Persson, D. Nilsson et S. Werner, «Heat Roadmap Europe 1: First Pre-Study for the EU27,» 2012.

[8] D. Connolly, B. V. Mathiesen, P. A. Østergaard, B. Møller, S. Nielsen, H. Lund, U. Persson, S. Werner, J. Grözinger, T. Boermans et others, «Heat Roadmap Europe 2: Second Pre-Study for the EU27,» 2013.

[9] S. Caird, R. Roy et S. Potter, «Domestic heat pumps in the UK: user behaviour, satisfaction and performance,» *Energy Efficiency,* vol. 5, pp. 283-301, Aug 2012.

[10] H. Wenju, J. Yiqiang, Q. Minglu, N. Long, Y. Yang et D. Shiming, «An experimental study on the operating performance of a novel reverse-cycle hot gas defrosting method for air source heat pumps,» *Applied Thermal Engineering,* vol. 31, pp. 363-369, 2011.

[11] F. Madonna et F. Bazzocchi, «Annual performances of reversible air-to-water heat pumps in small residential buildings,» *Energy and Buildings,* vol. 65, pp. 299-309, 2013.

[12] Y. Zhang, Q. Ma, B. Li, X. Fan et Z. Fu, «Application of an air source heat pump (ASHP) for heating in Harbin, the coldest provincial capital of China,» *Energy and Buildings,* vol. 138, pp. 96-103, 2017.

[13] K. Bakirci et B. Yuksel, «Experimental thermal performance of a solar source heat-pump system for residential heating in cold climate region,» *Applied Thermal Engineering,* vol. 31, pp. 1508-1518, 2011.

[14] H. ur Rehman, J. Hirvonen et K. Sirén, «A long-term performance analysis of three different configurations for community-sized solar heating systems in high latitudes,» *Renewable Energy,* vol. 113, pp. 479-493, 2017.

[15] P. Sporn et E. R. Ambrose, «The heat pump and solar energy proceedings of the world symposium on applied,» *Solar Energy,* vol. 11, pp. 1-5, 1955.

[16] J. Cai, J. Ji, Y. Wang et W. Huang, «Numerical simulation and experimental validation of indirect expansion solar-assisted multi-functional heat pump,» *Renewable Energy,* vol. 93, pp. 280-290, 2016.

[17] R. S. Kamel, A. S. Fung et P. R. H. Dash, «Solar systems and their integration with heat pumps: A review,» vol. 87, pp. 395-412, #jan# 2015.

[18] M. Mohanraj, Y. Belyayev, S. Jayaraj et A. Kaltayev, «Research and developments on solar assisted compression heat pump systems – A comprehensive review (Part A: Modeling and modifications),» *Renewable and Sustainable Energy Reviews* , pp. - , 2017.

[19] B. J. Huang et J. P. Chyng, «Integral-type solar-assisted heat pump water heater,» *Renewable Energy,* vol. 16, pp. 731-734, 1999.

[20] Z. M. Amin et M. N. A. Hawlader, «Analysis of solar desalination system using heat pump,» *Renewable Energy,* vol. 74, pp. 116-123, 2015.

[21] T. T. Chow, «A review on photovoltaic/thermal hybrid solar technology,» *Applied Energy,* vol. 87, pp. 365-379, 2010.

[22] S. A. Kalogirou, «Solar thermal collectors and applications,» *Progress in Energy and Combustion Science,* vol. 30, pp. 231-295, 2004.

[23] P. Bombarda, G. D. Marcoberardino, A. Lucchini, S. Leva, G. Manzolini, L. Molinaroli, F. Pedranzini et R. Simonetti, «Thermal and electric performances of roll-bond flat plate applied to conventional PV modules for heat recovery,» *Applied Thermal Engineering,* vol. 105, pp. 304-313, 2016.

[24] Q. Wang, Y.-q. Liu, G.-f. Liang, J.-r. Li, S.-f. Sun et G.-m. Chen, «Development and experimental validation of a novel indirect-expansion solar-assisted multifunctional heat pump,» vol. 43, pp. 300-304, #feb# 2011.

[25] A. Bridgeman et S. Harrison, «Preliminary experimental evaluations of indirect solar assisted heat pump systems,» chez *Proceedings of the 3rd Canadian solar building conference. Fredericton*, 2008.

[26] A. Loose, H. Drück, N. Hanke et F. Thole, «Field Test and Performance Monitoring of Combined Solar Thermal and Heat Pump Systems,» chez *ISES Solar World Congress, At Kassel, Germany*, 2011.

[27] Y. Bai, T. T. Chow, C. Ménézo et P. Dupeyrat, «Analysis of a Hybrid PV/Thermal Solar-Assisted Heat Pump System for Sports Center Water Heating Application,» *International*

Journal of Photoenergy, vol. 2012, 2012.

[28] X. Lv, G. Yan et J. Yu, «Solar-assisted auto-cascade heat pump cycle with zeotropic mixture R32/R290 for small water heaters,» *Renewable Energy,* vol. 76, pp. 167-172, 2015.

[29] J. Jie, C. Jingyong, H. Wenzhu et F. Yan, «Experimental study on the performance of solar-assisted multi-functional heat pump based on enthalpy difference lab with solar simulator,» *Renewable Energy,* vol. 75, pp. 381-388, 2015.

[30] A. Hepbasli et Y. Kalinci, «A review of heat pump water heating systems,» *Renewable and Sustainable Energy Reviews,* vol. 13, pp. 1211-1229, 2009.

[31] O. Ozgener et A. Hepbasli, «A review on the energy and exergy analysis of solar assisted heat pump systems,» *Renewable and Sustainable Energy Reviews,* vol. 11, pp. 482-496, 2007.

[32] B. Parida, S. Iniyan et R. Goic, «A review of solar photovoltaic technologies,» *Renewable and Sustainable Energy Reviews,* vol. 15, pp. 1625-1636, #apr# 2011.

[33] Y. Tian et C. Y. Zhao, «A review of solar collectors and thermal energy storage in solar thermal applications,» *Applied Energy,* vol. 104, pp. 538-553, 2013.

[34] L. Croci, L. Molinaroli et P. Quaglia, «Dual Source Solar Assisted Heat Pump Model Development, Validation and Comparison to Conventional Systems,» *Energy Procedia,* vol. 140, pp. 408-422, 2017.

[35] J. F. Chen, Y. J. Dai et R. Z. Wang, «Experimental and theoretical study on a solar assisted CO2\ heat pump for space heating,» *Renewable Energy,* vol. 89, pp. 295-304, 2016.

[36] M. D. Rosa, V. Bianco, F. Scarpa et L. A. Tagliafico, «Historical trends and current state of heating and cooling degree days in Italy,» *Energy Conversion and Management,* vol. 90, pp. 323-335, 2015.

[37] L. Keliang, J. Jie, C. Tin-tai, P. Gang, H. Hanfeng, J. Aiguo et Y. Jichun, «Performance study of a photovoltaic solar assisted heat pump with variable-frequency compressor – A case study in Tibet,» *Renewable Energy,* vol. 34, pp. 2680-2687, 2009.

[38] Y. H. Kuang et R. Z. Wang, «Performance of a multi-functional direct-expansion solar assisted heat pump system,» *Solar Energy,* vol. 80, pp. 795-803, 2006.

[39] G.-Y. Ma et H.-X. Zhao, «Experimental study of a heat pump system with flash-tank coupled with scroll compressor,» *Energy and Buildings,* vol. 40, pp. 697-701, 2008.

[40] G. K. Singh, «Solar power generation by PV (photovoltaic) technology: A review,» *Energy,* vol. 53, pp. 1-13, 2013.

[41] G. Bagarella, R. M. Lazzarin et B. Lamanna, «Cycling losses in refrigeration equipment: An experimental evaluation,» *International Journal of Refrigeration,* vol. 36, pp. 2111-2118, 2013.

768

769